Lab on a Chip

Devices and applications at the micro- and nanoscale

Accepted Manuscript

This article can be cited before page numbers have been issued, to do this please use: H. Nazari, A. Cho, D. Goss, J. P. Thiery and M. Ebrahimi Warkiani, *Lab Chip*, 2024, DOI: 10.1039/D4LC00296B.

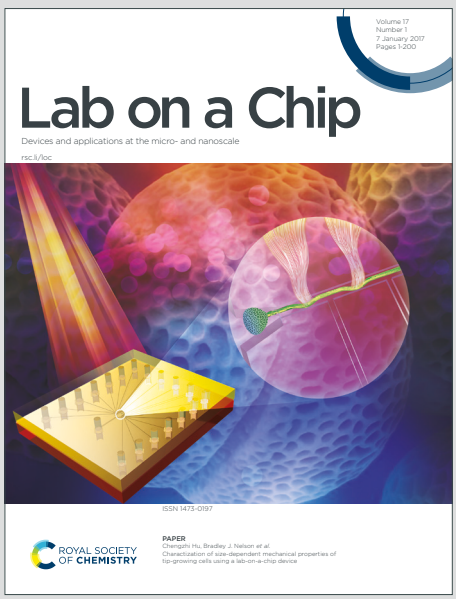

ROYAL SOCIETY OF CHEMISTRY

rsc.li/loc

View Article Online
DOI: 10.1039/D4LC00296B

The data produced and analyzed in this study are available from the corresponding author upon reasonable request. All data supporting the results of this study can be accessed in accordance with the journal's data-sharing policies.

Majid Ebrahimi Warkiani

Impact of Brain Organoid-Derived sEVs on Metastatic Adaptation and Invasion of Breast Carcinoma Cells through a Microphysiological System

View Article Online
DOI: 10.1039/D4LC00296B

Hojjatollah Nazari [a], Ann-Na Cho [b], Dale Goss [a], Jean Paul Thiery [c], Majid Ebrahimi Warkiani [a] *

[a] School of Biomedical Engineering, Faculty of Engineering and IT, University of Technology Sydney, Sydney, NSW, Australia
[b] School of Biomedical Engineering, Faculty of Engineering, The University of Sydney, Sydney, NSW, Australia
[c] UMR 7057 CNRS Matter and Complex Systems, Université Paris Cité, Paris, France

Contact: Prof. Majid Ebrahimi Warkiani (majid.warkiani@uts.edu.au). School of Biomedical Engineering, Faculty of Engineering and IT, University of Technology Sydney, Sydney, NSW, Australia

Abstract

Brain metastases are common in triple-negative breast cancer (TNBC), suggesting a complex process of cancer spread. The mechanisms enabling TNBC cell adaptation and proliferation in the brain remain unclear. Small extracellular vesicles (sEVs) play a crucial role in communication between breast carcinoma cells and the brain. However, the lack of relevant models hinders understanding of sEV-mediated communication. The present study assesses the impact of brain organoid-derived sEVs (BO-sEVs) on various behaviours of the MDA-MB-231 cell line, chosen as a representative of TNBC in a 3D microfluidic model. Our results demonstrate that 150-200 nm sEVs expressing CD63, CD9, and CD81 from brain organoid media decrease MDA-MB-231 cell proliferation, enhance their wound-healing capacity, alter their morphology into more mesenchymal mode, and increase their stemness. BO-sEVs led to heightened PD-L1, CD49f, and vimentin levels of expression in MDA-MB-231 cells, suggesting an amplified immunosuppressive, stem-like, and mesenchymal phenotype. Furthermore, these sEVs also induced the expression of neural markers such as GFAP in carcinoma cells. The cytokine antibody profiling array also showed that BO-sEVs enhanced the secretion of MCP-1, IL-6, and IL-8 by MDA-MB-231 cells. Moreover, sEVs significantly enhance the migration and invasion of carcinoma cells toward brain organoids in a 3D organoid-on-a-chip system. Our findings emphasize the potential significance of metastatic site-derived sEVs as pivotal mediators in carcinoma progression and adaptation to the brain microenvironment, thereby unveiling novel therapeutic avenues.

Keywords: Triple-negative breast cancer (TNBC), brain metastasis, brain adaptation, small extracellular vesicles (sEVs), organoid-on-a-chip, organoids

1. Introduction:

Distant metastases are the leading cause of death in many cancers, significantly reducing the 1-year survival rate of patients to 20% [1]. The brain frequently serves as a site for metastases in patients with breast cancer. Among the subtypes of breast carcinoma, triple-negative breast cancers (TNBC) are notably aggressive and are defined by their lack of estrogen and progesterone receptors, as well as the absence of human epidermal growth factor receptor-2 (HER2) expression on carcinoma cell surfaces. This subtype is associated with high recurrence rates and a propensity for metastasis to organs such as the brain [2, 3]. In advanced TNBC, approximately one-third of patients develop brain metastases, often as the initial sign of recurrence [4]. The incidence of brain metastases at the time of or after the diagnosis of metastatic TNBC ranges from 25% to 45% [5].

Brain metastases in breast carcinoma typically emerge several years to decades after the initial diagnosis, despite the early presence of circulating tumor cells in the bloodstream. This delayed manifestation suggests that brain colonization is a crucial phase in the metastatic sequence. The "seed and soil" hypothesis posits that a reciprocal interaction must be established between breast carcinoma cells and the neural microenvironment [6]. However, the mechanisms underlying the adaptation of breast carcinoma cells to the brain's ecosystem remain poorly understood.

Previous studies have shown that small extracellular vesicles (sEVs) play crucial roles in distant metastasis [7, 8]. sEVs are nano-sized biological carriers produced by cells, capable of transporting a wide range of signaling molecules, including RNAs and proteins, that play pivotal roles as messengers in human pathophysiology, including cancer metastasis [9-11]. The sEVs produced by carcinoma cells contribute to the development of metastatic niches in secondary organs [12-14]. Over the past decade, numerous studies on tumor-derived sEVs have investigated the impact of primary tumor-derived sEVs, known as "seed-derived sEVs," on tumor growth, progression, pre-metastatic niche formation, and metastasis [13, 15-18]. These studies have focused on the cross-talk between breast carcinoma cells and neural counterparts mediated by "seed" sEVs [19, 20]. However, the influence of 'soil-derived' sEVs on carcinoma cells has not been extensively investigated.

Metastatic carcinoma cells can be arrested in different zones of the brain, such as veins, venules, and even meninges, before breaching the blood-brain barrier (BBB). sEVs derived from the brain can intravasate through the BBB to modify carcinoma cells. Different types of brain cells, including neurons, astroglial cells, and microglia, are engaged in continuous communication. The impact of sEVs isolated from brain cells on the behaviour of breast carcinoma cells, such as tropism, adaptation, and invasion, remains unclear. Few studies have investigated the role of sEVs isolated from neuronal and glial cell lines on the behaviour of carcinoma cells, primarily in 2D environments. Breast carcinoma cells exhibiting increased brain tropism show downregulated expression of phosphatase and tensin homolog (PTEN) due to astrocytes through the NF-κB pathway [19]. The research demonstrated that sEVs released by astrocytes facilitate the transfer of microRNAs targeting PTEN to metastatic carcinoma cells. In contrast, depleting PTEN-targeting microRNAs in astrocytes or inhibiting the secretion of astrocyte-derived sEVs reverses the loss of PTEN and diminishes the brain metastasis of TNBC *in vivo* [19]. Furthermore, sEVs from astrocytes boost Reelin expression in Her2+ brain metastatic breast carcinoma cells, which results in the enhanced proliferation and survival of these carcinoma cells [21]. However, in these studies, astrocytes were cultured in 2D, which does not represent the 3D nature of human organs. Several studies have shown that the underlying mechanisms of sEVs in 2D and 3D conditions differ in terms of mechanical properties, production yield, and biomolecular content [22]. The 2D microenvironment fails to support complex interactions between neurons and glial cells, and 2D homogeneous cell cultures lack diversity in sEVs. Brain organoids, 3D miniature models of the human brain, mimic the structure and function of brain neurophysiology [23, 24]. Produced from embryonic stem cells (ESCs) or induced

pluripotent stem cells (iPSCs), brain organoids provide a more physiologically relevant environment of brain regions, including intricate crosstalk between neural cells [25, 26]. Therefore, brain organoids offer the opportunity to investigate the brain-specific microenvironment in sEV studies that can shed light on the adaptation and expansion of breast carcinoma cells within the brain environment.

In vitro and *in vivo* studies on clinical biopsies show that breast carcinoma cells exhibit neural traits and functions referred to as brain tropism and adaptation [27-29]. Breast carcinoma cells successfully metastasize to distant organs, contingent upon their ability to extravasate, evade immune surveillance, adapt, and proliferate to establish colonies in the brain's new microenvironment [30]. Recent studies indicate that breast carcinoma cells exhibit phenotypes of astrocytes, playing pivotal roles in their successful colonization [27, 28]. Metastatic breast carcinoma cells express N-methyl-D-aspartate (NMDA) receptors, allowing them to establish pseudo-tripartite synapses with neurons, thereby initiating glutamatergic signaling in a paracrine, peri-synaptic manner. Remarkably, these breast carcinoma cells inhabit the peri-synaptic niche traditionally occupied by astrocytes [29]. Once colonized in the brain, breast carcinoma cells express neuroligins and presynaptic neuronal neurexins, marking their phenotype adaptation. These components are critical for synaptic architecture [31, 32]. Additionally, breast carcinoma cells can express γ-aminobutyric acid (GABA) receptors after metastasizing to the brain. Consequently, these cells undergo dose-dependent proliferation in response to exogenous GABA, illustrating the complex interplay between neurotransmitters and carcinoma cell behaviours [33]. These adaptations may be facilitated by various interactions between carcinoma cells and the brain microenvironment, including neurotransmitters, hormones, interleukins, cytokines, growth factors, neurotrophic factors, sEVs, as well as direct cell-cell contacts, such as gap junctions and juxtracrine signaling [34-36]. However, the timing of breast carcinoma cell adaptation remains an open question. Some studies have focused on adaptation within the brain's microenvironment. Yet, this phenomenon has not been explored for cells residing in the brain's vascular and lymphatic systems before extravasation, where sEVs are the sole elements of adaptation that can easily traverse the BBB.

Herein, we aim to isolate and characterize sEVs from embryonic stem cell-derived brain organoids. Our *in vitro* studies investigate how these brain organoid-derived sEVs (BO-sEVs) influence the behavior of the TNBC cell line, affecting proliferation, morphology, adaptation, invasiveness, and stemness. We also elucidate the role of sEVs in promoting 3D migration and invasion of breast carcinoma cells toward brain organoids within a 3D microphysiological system. Additionally, we compare the effects of isolated BO-sEVs to both a control (no treatment) and the supernatant of brain organoids (BO-Media). This comparison helps to highlight the specific influence of sEVs among the various elements of the brain secretome that can pass the BBB.

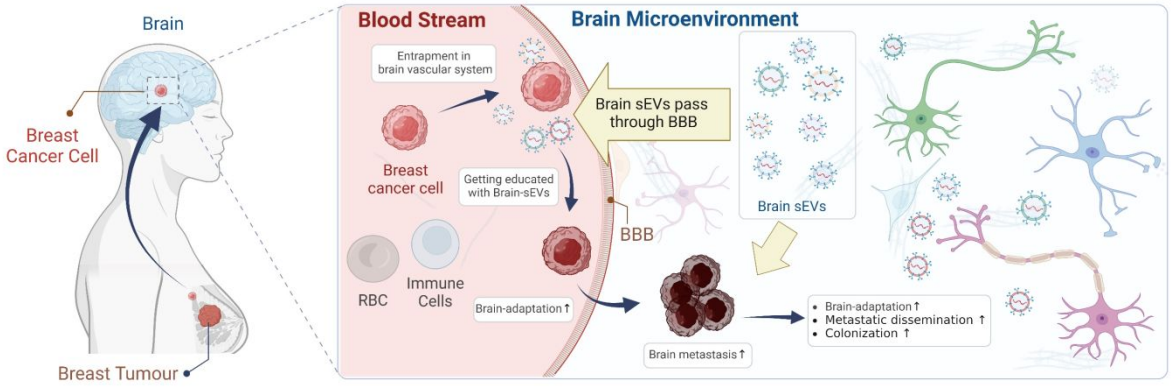

Graphical Abstract: *Illustrating the hypothesis on impact of brain sEVs on education and adaptation of breast carcinoma cells outside and then inside brain microenvironment. Figure created with Biorender.com.*

View Article Online
DOI: 10.1039/D4LC00296B

2. Materials and Methods:

2.1 Brain Organoid Culture and sEVs Isolation

2.1.1 Generating and Culturing Brain Organoids

Using previously reported standard protocols, brain organoids were generated using human embryonic stem cells (hESCs) [37]. Briefly, hESCs (H9; WIC-WA09-MB-001, WiCell) are grown on Matrigel-coated 6-well plates in minimal essential medium until they attain 80-90% confluence. After reaching this stage, the cells are washed with Dulbecco's Phosphate-Buffered Saline (DPBS) and exposed to StemPro Accutase Cell Dissociation Reagent at 37°C for one minute. These separated cells are then placed on AggreWell™ 800 plates with AggreWell EB Formation Medium supplemented with Y-27632. Following centrifugation, the cells are incubated at 37°C in a 5% CO_2 environment. After a day, the 3D embryoid bodies formed are transferred to ultra-low-attachment 10 cm dishes with Essential six medium, supplemented with SB-431542, dorsomorphin (Sigma-Aldrich, St. Louis, MO, USA), and XAV-939 to guide neuro-ectodermal differentiation. The medium is exchanged daily until the sixth day. On day six, the medium is replaced with a medium mixture of Neurobasal A (Cat No: 10888; Thermo Fisher Scientific), B-27 supplement (vitamin A-free), GlutaMax, Epidermal growth factor (EGF, Cat#236-EG; R&D Systems, USA), and essential fibroblast growth factor (bFGF) for neuronal differentiation. On day 24-day, the medium of Neurobasal A, B-27 (vitamin A-free), GlutaMax was supplemented with brain-derived neurotrophic factor (BDNF, Cat#78133; STEMCELL Technologies), and Human Recombinant Neurotrophin-3 (NT-3, Cat#78074; STEMCELL Technologies) for neuronal maturation. From days 43 to 200, the organoids are kept in a medium of Neurobasal A, B-27 (vitamin A-free), and GlutaMax (Thermo Fisher Scientific), excluding growth factors.

2.1.2 Isolating sEVs from Brain Organoid Media

Brain organoids medium was collected during 150-200 days of the culture period. sEVs isolation from collected medium was carried out through a series of centrifugation and ultracentrifugation steps. In brief, to remove dead cells, floating cells, and cellular debris, the brain organoid medium was subjected to several centrifugation steps at four °C using a HITACHI CR22N centrifuge (1200 rpm for 10 minutes, 2500 rpm for 15 minutes, and 8500 rpm for 30 minutes). The clarified supernatant was then filtered through a 0.22 µm sterile syringe filter (Merck Millipore, Burlington, MA, USA) and centrifuged again using an ultracentrifuge at four °C (17,500 rpm, 4F37L rotor, Sorvall WX ultra series, ThermoFisher, Waltham, CT, USA). The liquid phase was discarded, and the sEVs-containing pellet was diluted in 30 mL of sterile PBS. This solution was again centrifuged at 17,500 rpm for 150 minutes. The liquid was discarded, and the sEVs pellet was resuspended in 100 µL of sterile PBS and immediately preserved at -80°C.

2.1.3 Characterization of BO-sEVs

2.1.3.1 Transmission Electron Microscopy

BO-sEVs morphology is assessed using Transmission Electron Microscopy (TEM) for precise size and structure evaluation. In brief, five µL of brain organoid sEVs sample containing approximately 10^6 particles was fixed with 2.5% formaldehyde and applied onto 300-square mesh copper grids coated with a thin formvar carbon film. The grids were negatively stained using 1% UAR-EMS uranyl acetate replacement stain, incubated for 30 minutes, washed with PBS, and subsequently dried with filter paper. TEM imaging was conducted using a Tecnai T20 microscope operating at 200 kV and equipped with a Gatan 894 2 k × 2 k camera, capturing high-quality digital images.

2.1.3.2 Nanoparticle Tracking Analysis

Particle Metrix ZetaView® BASIC NTA - Nanoparticle Tracking Video Microscope PMX-120 (Particle Metrix, Meerbusch, Germany) was employed to study the size distribution and concentration of sEVs derived from brain organoids through Nanoparticle Tracking Analysis (NTA). For this analysis, parameters were set to target EVs specifically: a maximum area of 1000, a minimum area of 10, and a brightness threshold of 30. The sEVs used were diluted at 1:50 in Invitrogen's ultrapure distilled water. A 520 nm laser wavelength in scatter mode was used during the tracking process, scanning across 11 distinct positions.

2.1.3.3 Western Blotting

For western blotting, proteins from brain organoid derived-sEVs were isolated by lysing the sEVs using an equivalent amount of RIPA lysis and extraction buffer (89,900, Thermo Fisher, USA). The protein concentration was quantified using the Pierce BCA protein assay kit (Pierce Biotechnology, Waltham, CT, USA) per the manufacturer's guidelines. For the Western blot procedure, electrophoresis was conducted on ten µg of the sEVs protein using Bolt™ 4–12% Bis-Tris Plus Gels (NW04120BOX, Invitrogen, USA). These samples were combined with 4× Bolt™ LDS Sample Buffer (B0007, Thermo Fisher) and subjected to heating at 70°C for 10 minutes. The separated proteins were then moved to PVDF membranes (Thermo Fisher, USA). The membranes were blocked using 5% skim milk in PBS-T (PBS with 0.5% Tween-20) for a half-hour at ambient temperature, then treated overnight at four °C with primary antibodies targeting human CD63 (353,039 BioLegend, USA), human CD9 (312,102 BioLegend, USA), human CD81 (349,502, BioLegend, USA), L1CAM, GLAST, and LAMP1, all diluted 1:500 in PBS-T. The membranes were then exposed to HRP-tagged IgG secondary antibodies (diluted 1:2000) in PBS-T for 60 minutes at 37°C. After each treatment phase, membranes were rinsed thrice using the PBS-T buffer, each rinse lasting 10 minutes. The protein bands were made visible using the SuperSignal™ West Dura Extended Duration Substrate (37,071, Thermo Fisher, USA).

2.2 *in vitro* Assays on Breast Carcinoma Cells

2.2.1 Breast Carcinoma Cell Culture and Treatment

The MDA-MB-231 human breast adenocarcinoma cell line (ATCC, Cat#HTB-26, USA) was maintained in Dulbecco's Modified Eagle's Medium (DMEM) (Thermo Fisher Scientific, USA). This medium was enriched with 10% (v/v) fetal bovine serum (FBS) and a combination of 100 U/ml penicillin and 100 µg/ml streptomycin. Subsequently, the cells were exposed to either PBS, sEVs derived from brain organoids at a concentration of 50 µg/mL, or media from brain organoids for further experimentation.

2.2.2 Uptake of BO-sEVs by MDA-MB-231 Cells

The BO-sEVs were labelled with PKH-67(Sigma Aldrich, Cat#PKH67GL), a green fluorescent cell linker, and uptake assays were conducted in MDA-MB-231 cells using confocal microscopy. The labelling process was performed following the detailed protocol provided by the manufacturer (PKH-67 Green Fluorescent Cell Linker Kit, Sigma Aldrich). sEVs uptake and intracellular localization were carried out after 24 hours.

2.2.3 Proliferation Assay (MTT Assay)

The impact of brain-derived sEVs on the proliferation of MDA-MB-231 cells was assessed using the MTT assay. The assay was performed in a 96-well plate with a flat bottom, and the MTT Kit from Abcam (ab211091) was employed. The samples were prepared without FBS. The experimental procedure involved removing the cell culture media and adding 50 µL of MTT reagent along with 50 µL of media, followed by an incubation at 37 °C for 3 hours. Subsequently, 150 µL of MTT solvent

was added, and the plate was shaken at room temperature for 15 minutes. Optical density (OD) readings were taken at 590 nm on days 1, 2, 3, and 5 to determine the cellular metabolic activity.

2.2.4 Scratch Test and Morphological Studies

The scratch assay method was used to determine the impact of BO-sEVs after a 24-hour pre-treatment on MDA-MB-231 cell migration. 8×10^4 MDA-MB-231 cells were seeded per well in a 24-well plate and cultured in DMEM with 5% FBS, at 37°C and 5% CO2 until they achieved 90-95% confluency. After reaching this density, the existing medium was replaced with DMEM devoid of FBS. The cells were then washed twice with PBS after removing the FBS-free medium. Using a sterile 200 µL pipette tip, a straight scratch was made across the cell layer. Following another PBS wash, the migratory behaviour of MDA-MB-231 cells pre-treated with either PBS, BO-sEVs at a concentration of 50 µg/mL, or Brain organoid supernatant media (BO-Media), was observed over 24 hours using an Olympus phase-contrast microscope. The scratch widths and migration speeds were then quantified using Image J software (version 1.46), with data being adjusted based on the respective control groups. We evaluated cell circularity and aspect ratio using ImageJ to analyse cell morphology. The circularity metric was calculated as circularity = $4\pi(\text{area}/\text{perimeter}^2)$. This equation was applied to ten chosen digital images showcasing all MDA-MB-231 cell groups. A value of 1.0 for circularity corresponds to an ideal circle, while values approaching 0.0 correspond to increasingly elongated shapes.

2.2.5 Immunostaining Imaging and Image Analysis

On day 200, the brain organoids underwent fixation in a 4% paraformaldehyde solution for an overnight period at 4°C, followed by two PBS washes. They were then sequentially submerged in 15% and 30% (w/v) sucrose solutions prepared with distilled water, each for four hours at 4°C with rotation, for cryoprotection. Afterwards, the organoids were encased in OCT compound and frozen at −80°C. These samples were then cut into 20 µm thick tissue sections using a cryostat (Leica Inc., Wetzlar, Germany). For immunohistochemical analysis, the tissue sections were first rinsed with PBS to eliminate any residual OCT and then permeabilized with 0.5% (v/v) Triton X-100 (Cat#X100; Sigma-Aldrich) in PBS for 60 minutes. Subsequently, the sections were incubated with 5% (w/v) bovine serum albumin (Cat#216006980; MP Biomedicals, Santa Ana, CA, USA) for five hours to prevent non-specific antibody binding. Finally, 100 µL of the primary antibody was applied to the sample, which was then covered with parafilm and left to incubate overnight at 4°C. After washing three times with PBS, 100ul of secondary antibodies were added to the samples and covered with parafilm RT for 3 hours. After washing with PBS, DAPI was added to the samples at room temperature for 30min.

Immunostaining techniques were used to study the impact of sEVs originating from brain organoids on the expression of various markers related to cancer progression, stem cell attributes, and neural properties.8×10^4 MDA-MB-231 cells were plated in a glass-bottom µ-Dish (35 mm, ibidi) and allowing their growth in DMEM enriched with 5% FBS at 37°C and 5% CO2 until they reached about 70-75%confluency. Cells were cultured overnight in DMEM without FBS prior to treatment. Thereafter, cells were cultured in either PBS, sEVs sourced from brain organoids (at protein concentrations of 25 and 50 µg/mL), or the supernatant medium of brain organoids (BO-Media) for 24 hours.

Subsequently, the cells were fixed using 4% paraformaldehyde (PFA) (Sigma-Aldrich, St. Louis, MO, USA) for 30 minutes at room temperature. A 0.1% Triton-X 100 (Sigma-Aldrich, St. Louis, MO, USA) solution was applied to the cells for 10 minutes for permeabilization. To block non-specific binding, the cells were treated with 1.5% BSA (Sigma-Aldrich cat no.: A5611) for two hours. This was followed by staining the cells with anti-human CD44 (1:200, Abcam, Cat# ab194988), anti-human PD-L1(1:200, Abcam Cat#ab214958.), anti-human CD49f (1:500 Alexa Fluor® 488, Biolegend,

Cat#313608), anti-human EGFR (1:500 PerCP/Cyanine5.5, Biolegend, Cat#352914), and anti-human Vimentin (1:500, Biolegend, Cat# 677804) and anti-human GAD2/GAD65 (Cat#AF2247,R&D), anti-human GFAP (Cat#G9269, Sigma), Phalloidin Atto 565 (Sigma, Cat#94072), anti-human Ki-67 (1:250, Abcam, Cat#15580) and anti-human MAP2 (Cat#M3696, Sigma). Imaging of the samples was performed using a Leica Stellaris 8 confocal microscope. The intensity of the fluorescent signal, serving as an indicator of protein expression, was quantified using Image J software (version 1.46).

2.2.5.1 Proteomics Sample Preparation for LC-MS/MS

MDA-MB-231 cells exposed to PBS, sEVs from brain organoids, and supernatant from brain organoids underwent three successive washes with PBS. After this, the cells were lifted using a cell scraper and subjected to another triple washing with PBS. These samples then underwent a sonication process, maintaining an active cycle of 30 seconds followed by passive cycle of 10 seconds on ice.

The sample treatment procedure was modified based on the method involving STAGE Tips outlined in a prior study [38]. In summary, approximately 1 µl (around 50 µg of protein, as determined by BCA assay) of lysed sEVs/cells was mixed with lysis buffer (containing 50 mM Tris–HCl pH 8.8, 1% sodium deoxycholate, 5 mM Tris (2-carboxyethyl) phosphine hydrochloride as a reducing agent, and 20 mM acrylamide monomers as an alkylation agent) in a 1:25 ratio, then heated at 95 °C for 5 minutes. This process facilitated protein denaturation, reduction, and alkylation. Proteins were subsequently digested using sequencing-grade trypsin (1 µg/µl; Promega, USA) at 37 °C overnight, maintaining an enzyme to substrate ratio of 1:50. Digestion was stopped by adding an equal volume of ethyl acetate with 1% trifluoroacetic acid (TFA). Peptide mixtures were purified, concentrated, and enriched using a STAGE Tip, prepared from a 47 mm styrene divinyl benzene-reversed phase sulfonate (SDB-RPS Empore, 3 M) disk core, extracted and placed into a 100 µl pipette tip. After vigorous vortex mixing, ~10 µg of digested peptides were applied to the STAGE Tip, washed with 99% ethyl acetate + 1% TFA, and eluted with 5% ammonium hydroxide + 80% acetonitrile. The eluates were dried in a SpeedVac and resuspended in 0.1% formic acid to a final concentration of 0.4 µg/µl.

Peptide samples were loaded onto a nanoEase Symmetry C18 trapping column using an Acquity M-class nanoLC system (Waters, USA), then transferred to a picofrit column packed with SP-120-1.7-ODS-BIO resin, maintained at 45 °C. Peptides were eluted into a Q Exactive Plus mass spectrometer (Thermo Scientific) with a gradient program and ionized at 2400 V. A data-dependent MS/MS experiment was conducted, selecting the Top 12 peptides for fragmentation, with specific settings for the survey scan, fragmentation, and scan resolution. Precursor peptide masses were excluded for 30 seconds post-analysis.

2.2.5.2 Proteomics Data Analysis

The mass spectrometry (MS/MS) data was analysed using the Peaks Studio X Pro software, referencing both the 2019 human proteome and a standard contaminants database. The analysis parameters were set as follows: no fixed modifications, variable modifications to propionamide, oxidized methionine, and deamidated asparagine. The enzyme specified was semi-trypsin with an allowance for up to 3 missed cleavages. The peptide mass had a tolerance of 10 ppm, while the MS/MS mass was set at a tolerance of 0.05 Da. Search results were refined to only consider peptides with a –log10p score correlating with a False Discovery Rate (FDR) of less than 1%, the threshold where matches from the decoy database constituted less than 1% of the total. For label-free quantification, the PEAKS Q module was utilized.

View Article Online
DOI: 10.1039/D4LC00296B

2.3 Cytokine Profiling Assays on sEVs Treated Samples

The culture media from devices exposed to sEVs were examined with the Human Cytokine Antibody Array (Abcam, Cat# ab133997, Cambridge, UK), adhering to the manufacturer's instructions. In brief, the culture medium, collected from samples initially treated with PBS and 50 µg/mL BO-sEVs, was centrifuged and then subjected to overnight hybridization on the array membrane at four degrees Celsius. Subsequent to washing the membrane, an anti-cytokine secondary antibody was applied. Cytokine detection was achieved by the addition of HRP-conjugated streptavidin to the membrane. The intensity of the signals from each cytokine spot on the membrane was measured using ImageJ software.

2.3.1 Co-culture Experiment in Microfluidic Devices

A microfluidic device (DAX01-1PAK, Singapore). This microfluidic device consists of parallel two media channels, called gel channel, to fill with an extracellular gel matrix of collagen type I. A 200 µl collagen gel solution (2.5 mg/ml) was prepared on ice by mixing 20 µl of 10X PBS, four µl of 0.5 N NaOH, 160 µl of collagen type I (Corning), and 10 days-old brain organoids in ten µl of brain organoid medium. The collagen solution, including the brain organoids, was subsequently injected into the microfluidic middle channel device. The device was then transferred to a cell culture incubator at settings of 37°C and 5% CO_2, allowing for a 40-minute period to enable gel polymerization via thermal solidification. Once the gel was polymerized, a combined media (a 1:1 mix of serum-free brain organoids and FBS-free DMEM media) was added to the appropriate medium channels. In the case of the migration assay, MDA-MB-231 cells were infused into the side channels, according to the manufacturer's guidelines.

To assess the viability of brain organoids during the experiment inside the chip, the Live/Dead staining solution was prepared by diluting the Live/Dead Kit components (Calcein AM and ethidium homodimer-1, ThermoFisher, Cat# L3224) in sterile PBS, following the manufacturer's instructions.

2.3.2 Immunostaining of Cells *In situ* in the Chip

Media from the microfluidic devices was discarded, and an initial wash was performed using cold PBS. For this wash, 70 µl of the solution was introduced into one port, followed by an addition of 50 µl into the corresponding port on the other side of the medium channel. Afterward, the specimens were stabilized using 4% paraformaldehyde (PFA) (Sigma-Aldrich, St. Louis, MO, USA) for 15 minutes at ambient temperature. The fixed samples were then treated with a 0.1% Triton-X 100 solution (Sigma-Aldrich, St. Louis, MO, USA) and left for 10 minutes. For two hours, A blocking phase was conducted using 1.5% BSA (Cat# A5611, Sigma-Aldrich, St. Louis, MO, USA). Once blocked, staining was performed to identify PAX6 (1: 500, Cat# 901301, Biolegend) and Vimentin markers (1:200, Cat#677804, Biolegend) to study their localization and prevalence cells.

2.4 Statistical Analysis

The quantitative data obtained from experiments were analyzed and presented as mean ± standard error of the mean (SEM). Statistical analyses were conducted using the Student's t-test. Statistical significance was defined as a p-value < 0.05. Microscopic images presented in the study are representative images derived from three independent experimental replicates.

3. Results

3.1 Generation and Characterization of Brain Organoids

Brain organoids were generated from hESCs using a published protocol [37] and were used as a source of sEVs on day 200 (Figure 1A). The hESCs were seeded into AggreWellTM platforms to generate embryonic bodies, and then early brain organoids were formed in one day with sizes ranging

View Article Online
DOI: 10.1039/D4LC00296B

between 200-300 µm (Figure 1B). The early organoids were then transferred to non-adherent Petri dishes (Figure 1C) and cultured for differentiation and maturation. The organoid's diameters were gradually increased from 2 mm at day 30 to 8-10 mm by days 150-200, showing the successful development of the brain organoid generated from hESCs (Figure 1D). Immunostaining of brain organoid sections showed that the organoids matured by day 200, as evidenced by the presence of glial fibrillary acidic protein (GFAP) astrocyte marker, and, the Microtubule-associated protein 2 (MAP2) neuronal marker, suggesting the development of astroglial and neuronal cell populations at day 200 of culture (Figure 1E-J). We collected the medium from the brain organoids and isolated the sEVs for the following assays. The detailed cellular architecture within the organoids was highlighted by the distinct expression patterns of GFAP and MAP2, denoting the organoid's complex cellular composition resembling brain tissue.

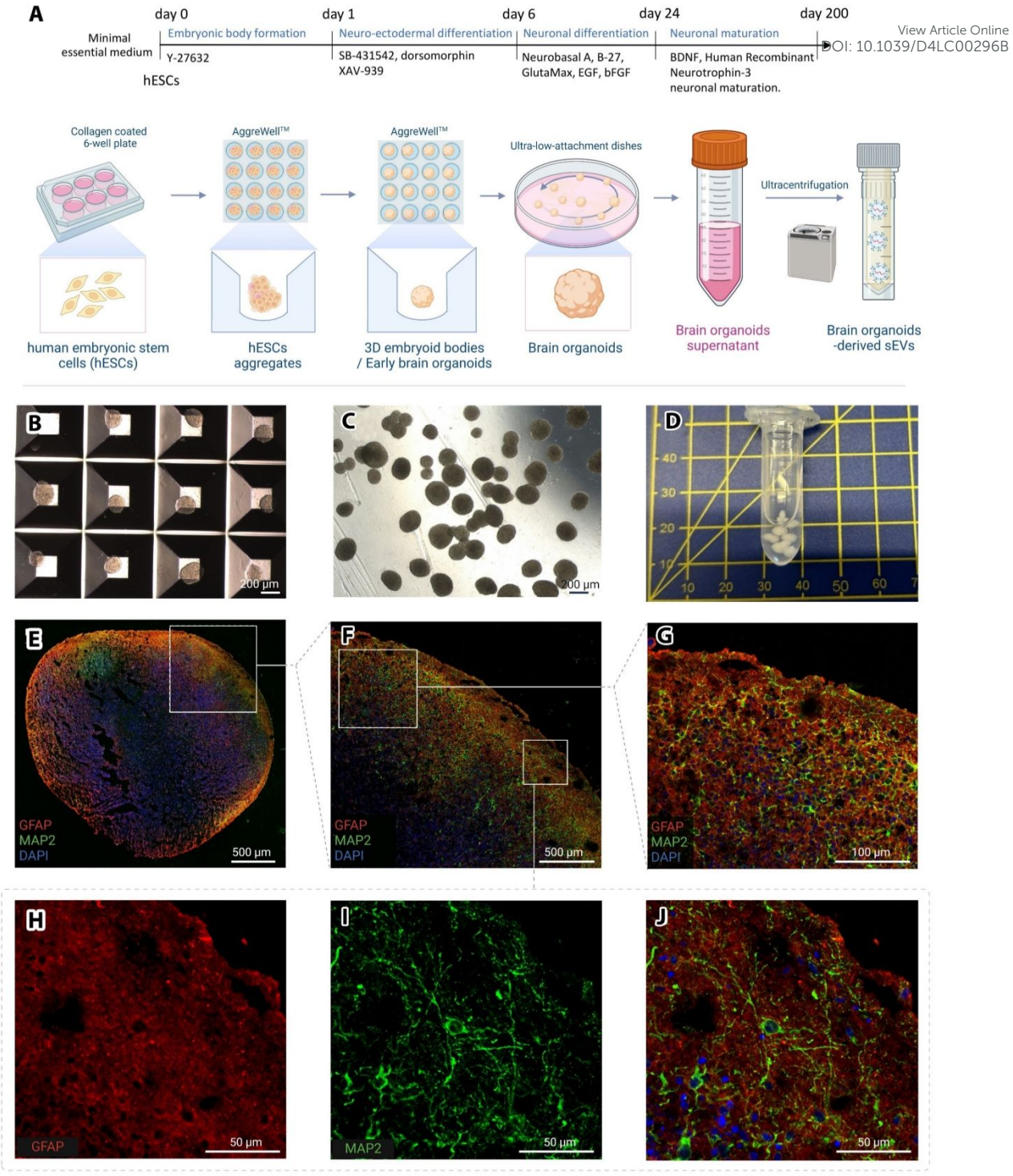

Figure 1. *(A) Schematic of the timeline and steps for generating human brain organoids (BO) from human embryonic stem cells (hESCs). BO-sEVs were isolated from the supernatant of brain organoids. Figure created with BioRender.com. Microscopic images depict early-stage brain organoids inside microwells (B) and a Petri dish (C). (D) Macroscopic image illustrates matured brain organoids on day 200. Confocal images show an hESC-derived brain organoid section on day 200, stained for astrocytes (GFAP, red), neurons (MAP2, green), and nuclei (DAPI, blue) at 10X magnification. The dispersion of neurons (stained with MAP2, green) through astrocytes (stained with GFAP, red) is depicted at 40X (G) and 63X (H-J) magnification. Scale bars: B and C, 200 µm; E and F, 500 µm; G, 100 µm; H-J, 50 µm.*

3.2 Characterization of sEVs

sEVs were isolated from the brain organoid conditioned medium on days 150-200. TEM, NTA, western blotting, and proteomics were used to characterize the BO-sEVs in terms of size, morphology, and protein content. TEM images of the BO-sEVs evidenced their spherical shape with an average diameter of 147.97 ± 33.75 nm (Figure 2A). NTA showed that the sEVs reached a concentration of 1.2 x 10^10 particles/mL and a median size of 157.1 ± 99 nm (Figure 2B). Western blot analysis demonstrated the presence of tetraspanins family members such as CD9, CD63, and CD81 within the sEVs (Figure 2C). Results also show that GLAST (Glutamate Aspartate Transporter) and LAMP1 (Lysosomal-Associated Membrane Protein 1) were expressed in the BO-sEVs (Figure 2C).

Proteomics data provided an extensive protein profiling of the BO-sEVs. The top 20 proteins, included a central nervous system-related proteins including NEP (Neprilysin), PRDX6 (Peroxiredoxin 6), ANXA1 (Annexin A1), GDIB (Guanine nucleotide dissociation inhibitor beta), and HSP90A (Heat shock protein HSP 90-alpha) (Figure 2D). Furthermore, proteins that are associated with progression of TNBC were identified; they include RALB (Ras-related protein Rab-11B), GSTP2 (Glutathione S-transferase pi-2), CDK18 (Cyclin-dependent kinase 18), RAB2A (Ras-related protein Rab-2A), and CDC42 (Cell division control protein 42 homolog) (Figure 2D).

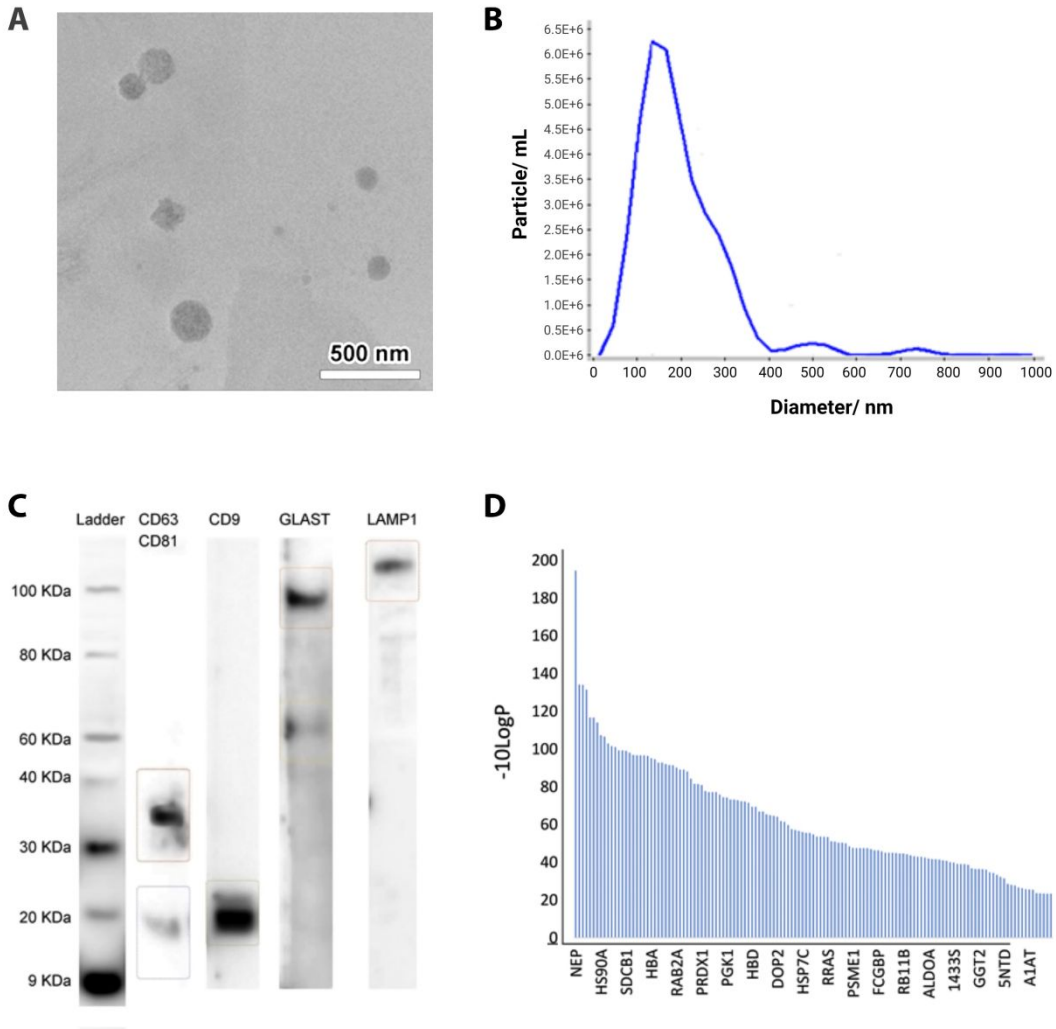

Figure 2. *Characterization of BO-sEVs by TEM, NTA, Western blotting, and Proteomics. A) TEM micrographs show the morphology, structure, and size of BO-sEVs. B) NTA histogram of BO-sEVs. C) Western blot of BO-sEVs for sEVs biomarkers including CD63, CD81, CD9, GLAST, and LAMP1. D) Proteomics analysis of BO-sEVs. Scale bar, A: 500 nm.*

View Article Online
DOI: 10.1039/D4LC00296B

3.3 Uptake assay of Brain Organoid derived-sEVs and Impact on MBA-MB-231 Cell Proliferation

BO-sEVs labelled with PKH-67 were internalized by MDA-MB-231 cells. We examined the uptake dynamics of these fluorescently labelled sEVs showing that MDA-MB-231 cells captured the sEVs after a 24-hour incubation period (Figure 3 A). A fluorescence-based quantitative analysis of fluorescence intensity revealed a mean value of 14.231 ± 1.458, reflecting the extent of sEVs uptake. We investigated the effect of brain-derived sEVs on the proliferation of MDA-MB-231 cells using the MTT assay. There compared the proliferation of three groups: a control group with no treatment, a group treated with 50 µg/mL BO-sEVs, and a group treated with brain organoid supernatant (BO-Media, 50 µg/mL protein). In the control group, cell growth consistently increased over three days (Figure 3Bi). results show that on day 3, the sEVs caused a significant decrease in OD and viability of MDA-MB-231 cells compared to the control (Figure 3Bii). Conversely, the group exposed to brain organoid media showed increased growth compared to the control and sEVs-treated groups. The measurements increased continuously on day 5. These findings demonstrate the inhibitory effect of BO-sEVs on the growth of MDA-MB-231 cells in a 5-day period.

3.4 Impact of BO-sEVs on MDA-MB-231 Cells Spreading Dynamics and Morphology

The wound-healing assay was used to assess the impact of BO-sEVs on in the migration ability of MDA-MB-231 cells (Figure 3 C-E). There were three groups: a control group with no treatment, a group treated with 50 µg/mL BO-sEVs, and a group of BO-Media (50 µg/mL). The cell migration area of BO-sEVs group was 786.27 ± 265.46 µm^2, whereas the control group was (94.36 ± 252.49 µm^2 which implied a significant reduction in BO-sEVs group. This reduction suggests enhanced cell flattening, triggered by BO-sEVs. Conversely, the Brain Organoid Media group exhibited a minor decrease in mean wound area (512.13 ± 157.62 µm^2) compared to the BO-sEVs group, although the difference was not statistically significant (NS).

Phenotypes of MDA-MB-231 cells were described by assessing circularity and aspect ratio using image analysis. The control group displayed a mean circularity value of 0.306 ± 0.070, while cells treated with BO-sEVs and brain organoid media exhibited a significant decrease in circularity to 0.231 ± 0.066 and 0.201 ± 0.039, respectively (Figure 3 G). The aspect ratio of MDA-MB-231 cells in the control group showed a mean value of 3.426 ± 0.972, which increased significantly to 5.740 ± 1.580 and 6.316 ± 1.991, respectively, in the BO-sEVs group and Brain Organoid Media group (Figure 3 H).

Figure 4. A demonstrates that treatment of MDA-MB-231 cells with BO-sEVs and BO-media enhanced the elongation of MDA-MB-231 cells. Results also shows that sEVs changes the uniformity, distribution, and alignment of actin filaments spanning across the cell (Figure 4A) . Specially the presence of stress fibres is visible in BO-sEVs group. Confocal imaging and quantitative analysis of Ki-67 staining showed a significant reduction in the proportion of Ki-67 positive cells following 48-hours treatment with BO-sEVs, indicating a negative impact of BO-sEVs on cell proliferation (Figure 4B-C).

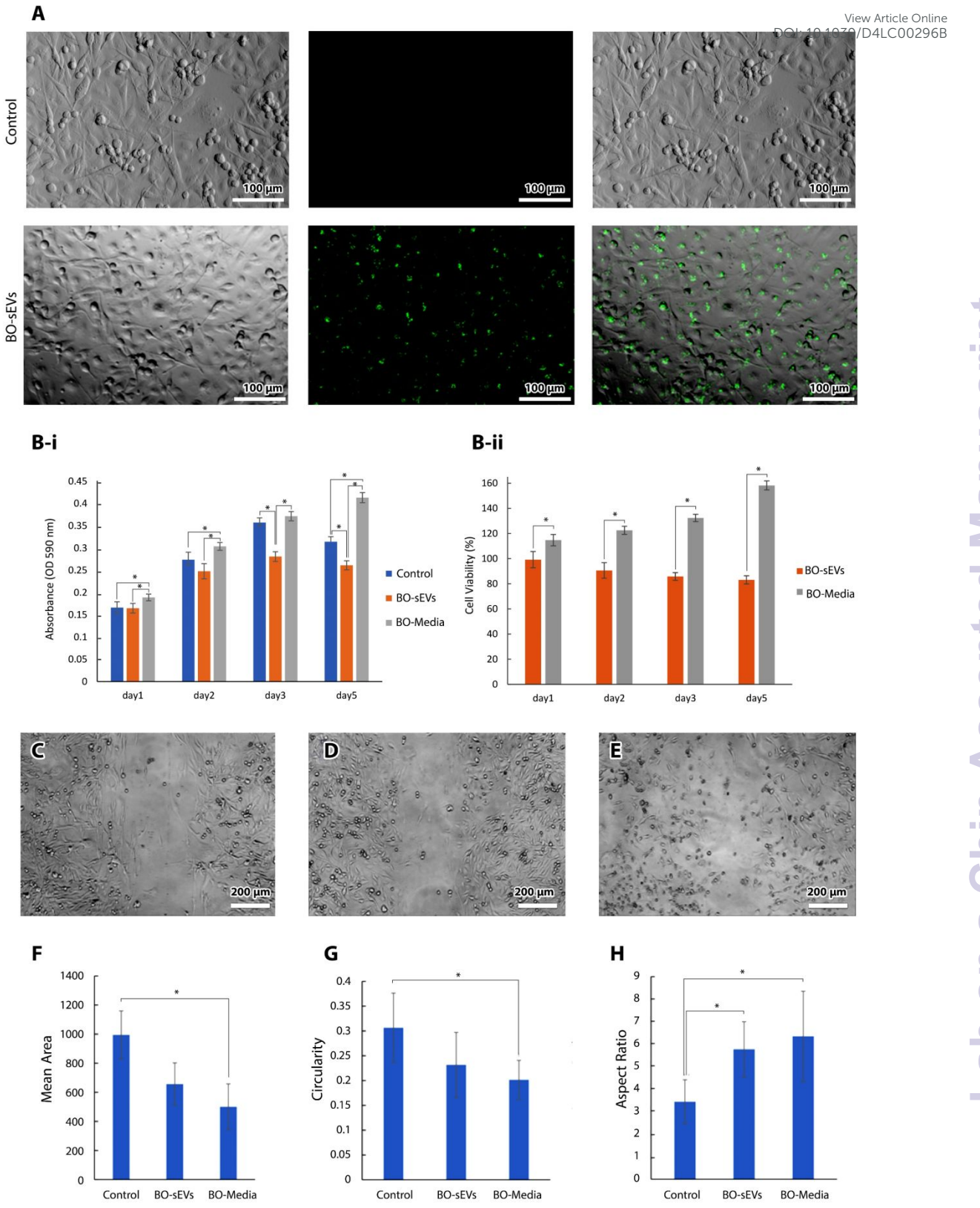

Figure 3. *A) Confocal microscopy shows the uptake of PKH-67-conjugated BO-sEVs by MDA-MB-231 cells following a 24-hour treatment (green: PKH-67-sEVs, Scale bar: 100 µm). Bi-Bii) MTT assay of MDA-MB-231 cells treated with BO-sEVs on days 1, 2, 3, and 5 (*p < 0.05). Scratch test on MDA-MB-231 cells treated with (C) PBS as control, (D) BO-sEVs, and (E) brain organoid media (Scale bar: 400 µm). Analysis of MDA-MB-231 cells post 24-hour treatment for (H) mean area, (I) circularity, and (J) aspect ratio, following treatment with PBS, BO-sEVs, and brain organoid media (*p < 0.05).*

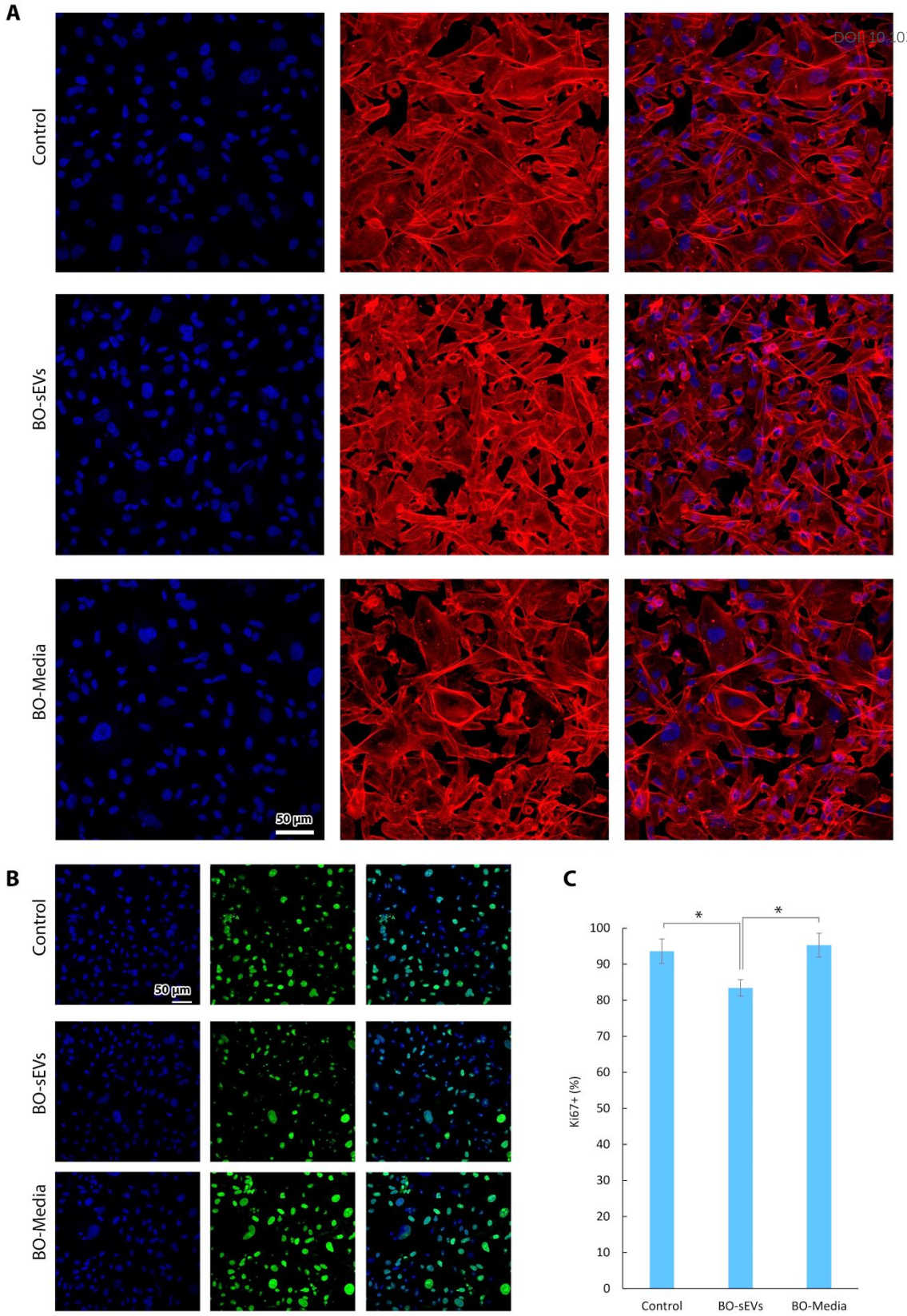

Figure 4. *(A) Confocal microscopy images of MDA-MB-231 cells immunostained with Phalloidin (F-Actin, red) and DAPI (nucleus). These images illustrate the orientation and morphology of F-actin fibers in MDA-MB-231 cells at 20X magnification across control, BO-sEVs, and BO-Media groups. (B) Confocal imaging depicts the expression levels of Ki-67 (green) in the nuclei (blue, DAPI) of MDA-MB-231 cells treated with PBS, BO-sEVs, and BO-Media (*p < 0.05). Scale bars: A and B, 50 µm.*

3.5 BO-sEVs Induced Sphere Formation of Breast Carcinoma Cells

The spheroid formation assay investigated the impact of sEVs from brain organoids on the 3D spheroid-forming ability of MDA-MB-231 cells in three-dimensional culture. MDA-MB-231 cells were cultured in non-adherent Petri dishes and treated with BO-sEVs (final concentration of 50 µg/mL in FBS-free medium) for seven days. Our results showed that the average diameter of MDA-MB-231 spheroids increased from 129.851 ± 59.323 µm to 205.421 ± 132.029 µm after incubation with BO-sEVs (Figures 5A-C). Immunostaining data show the expression of CD44, as a stemness marker was significantly increased in MDA-MB-231 cells spheroid after incubation with BO-sEVs (Figures 5D and E). Conversely, the expression of E-cadherin, as the most known epithelial marker, in MDA-MB-231 spheroids decreased after treatment with BO-sEVs (Figures 5F and G). These data suggest that BO-sEVs promote stemness and invasive properties in MDA-MB-231 spheroids.

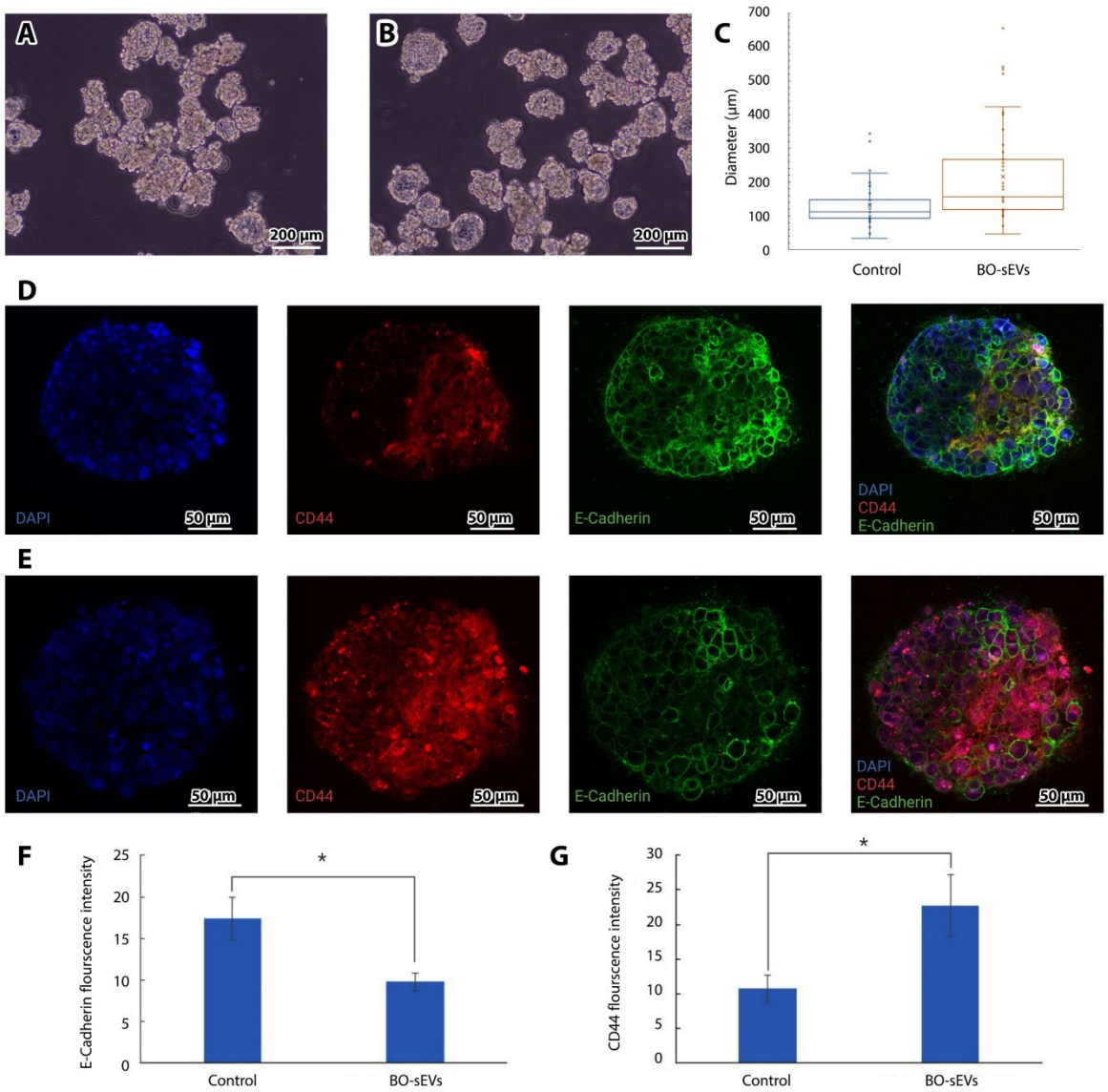

Figure 5. *Microscopic images of MDA-MB-231 spheroids at day 9, without (A) and with (B) the treatment of BO-sEVs. (C) Treatment with BO-sEVs significantly increased the size of generated spheroids. Confocal imaging of nuclei (DAPI, blue) CD44 (red) and E-cadherin (green) in MDA-MB-231 spheroids treated with (D) PBS (control) and (E) BO-sEVs over a 7-day period. Quantitative analysis of mean fluorescence intensity of (F) E-cadherin and (G) CD44 (*p < 0.05) in MDA-MB-231 spheroids. Scale bars: A and B, 200 µm; D and E, 50 µm.*

3.6 BO-sEVs Modifies Breast Carcinoma Cell Behaviours

The expression of four distinct markers involved in tumor immune evasion, epithelial cell adhesion, EMT, and EGFR signaling was assessed in MDA-MB-231 cells treated with BO-sEVs or conditioned media. BO-sEVs significantly increased the expression of programmed death-ligand 1 (PD-

View Article Online
DOI: 10.1039/D4LC00296B

L1), CD49f, and vimentin in MDA-MB-231 cells (Figure 6A-C). Notably, the BO-sEVs group exhibited significantly higher PD-L1 expression compared to the control group, suggesting potential modulation of the immune response (Figure 6C). Similarly, CD49f expression was significantly elevated in the BO-sEVs group compared to the control, indicating enhanced mesenchymal properties (EMT) and stemness (Figure 6D). Furthermore, the BO-sEVs group displayed significantly higher vimentin expression compared to the control, potentially reflecting changes in mesenchymal characteristics (Figure 6E). No significant differences in epidermal growth factor receptor (EGFR) expression were observed among the groups (Figure 5F).These data suggest roles for BO-sEVs in immune evasion, adhesiveness, and stemness induction in breast carcinoma cells after a 24-hour incubation.

View Article Online
DOI: 10.1039/D4LC00296B

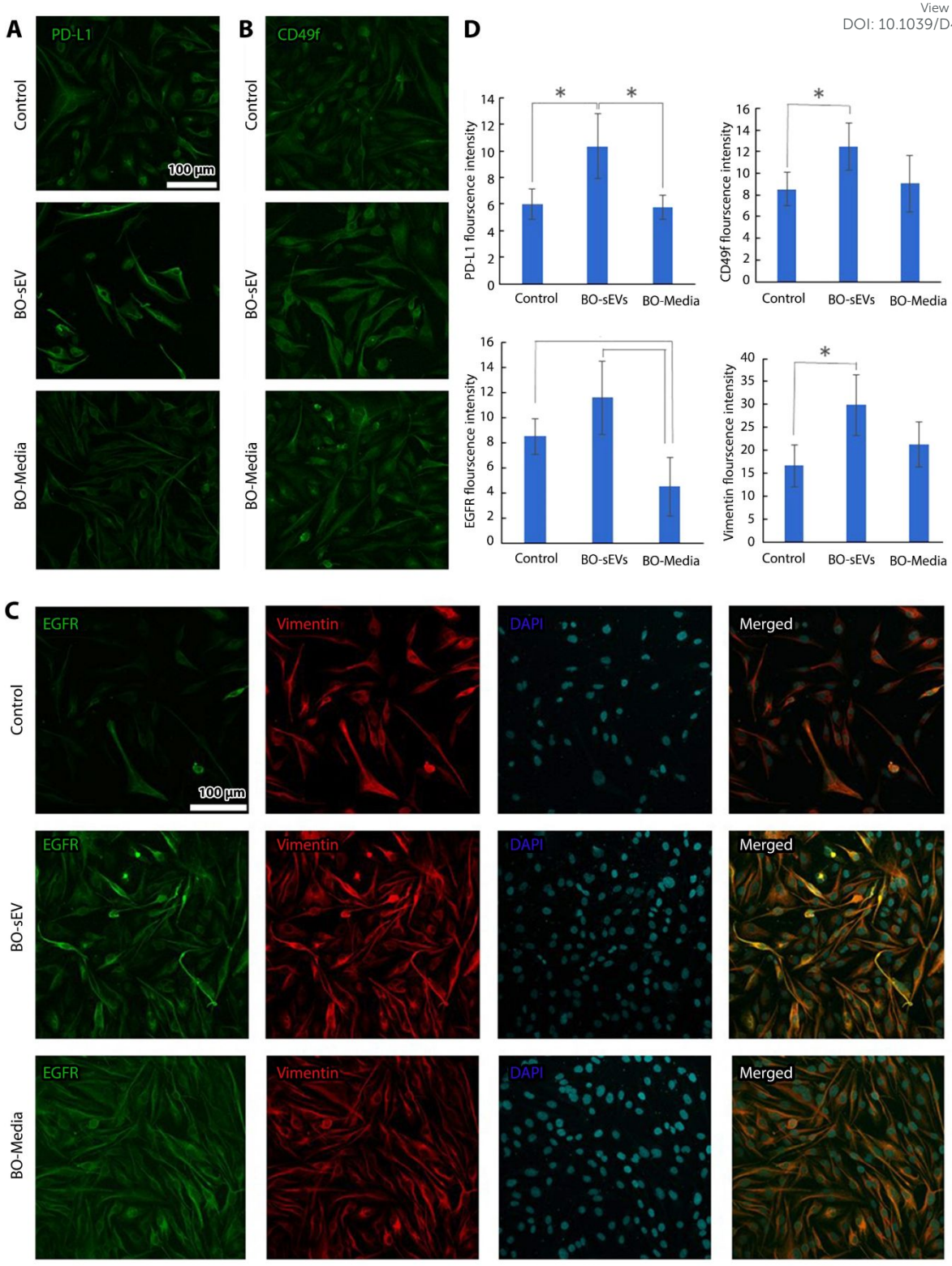

Figure 6. *Immunostaining images showing the expressions of PD-L1 (A), CD49f (B), and EGFR-vimentin (C) in MDA-MB-231 cells treated with PBS (control), BO-sEVs, and brain organoid media after 24 hours (Scale bar: 100 µm). Mean fluorescence analysis showed that BO-sEVs significantly increased the expression of PD-L1, CD49f, and vimentin in breast carcinoma cells (*p < 0.05).*

3.7 BO-sEVs Enhanced Expression of Glial and Neuronal Markers in Breast Carcinoma Cells

View Article Online
DOI: 10.1039/D4LC00296B

Immunostaining data revealed enhanced expression of glial and neuronal markers in MDA-MB-231 cells by incubating with BO-sEVs for 24-hours. In this step we used one more concentration of sEVs (25 µg/mL) to see if the lower concentration of sEVs also induce the expression of neural markers in breast carcinoma cells. Therefore, the study included four experimental groups: control, 25 µg/mL BO-sEVs, 50 µg/mL BO-sEVs, and brain organoid media.

In vitro studies have shown that breast carcinoma cells express neuronal and glial markers (Figure 7A). Glutamic Acid Decarboxylase 65 (GAD65), an enzyme involved in the generation of GABA neurotransmitters, and Microtubule-Associated Protein 2 (MAP2), a structural protein, are neuronal markers in the brain. Our results showed that the expression of GAD65 marker had a basal level of 1.191 ± 0.651 in the control group. Exposure to 25 µg/mL sEVs induced a significant elevation to 9.957 ± 2.136, with a further increment observed in the 50 µg/mL sEVs group (10.210 ± 2.584). Notably, the brain organoid media demonstrated the highest level (20.197 ± 5.654) in the expression of GAD65 (Figure 7B). The GFAP marker exhibited an increased expression, from 0.968 ± 1.1 in the control to 8.446 ± 2.192, 15.264 ± 3.979, and 13.460 ± 4.024 in the respective treatment groups (Figure 7C). Similarly, the expression of MAP2 displayed a consistent pattern, transitioning from 0.968 ± 1.1 in the control to 10.003 ± 2.725, 12.440 ± 3.939, and 11.680 ± 2.557, respectively, in the 25 µg/mL BO-sEVs, 50 µg/mL BO-sEVs, and brain organoid media groups (Figure 7D).

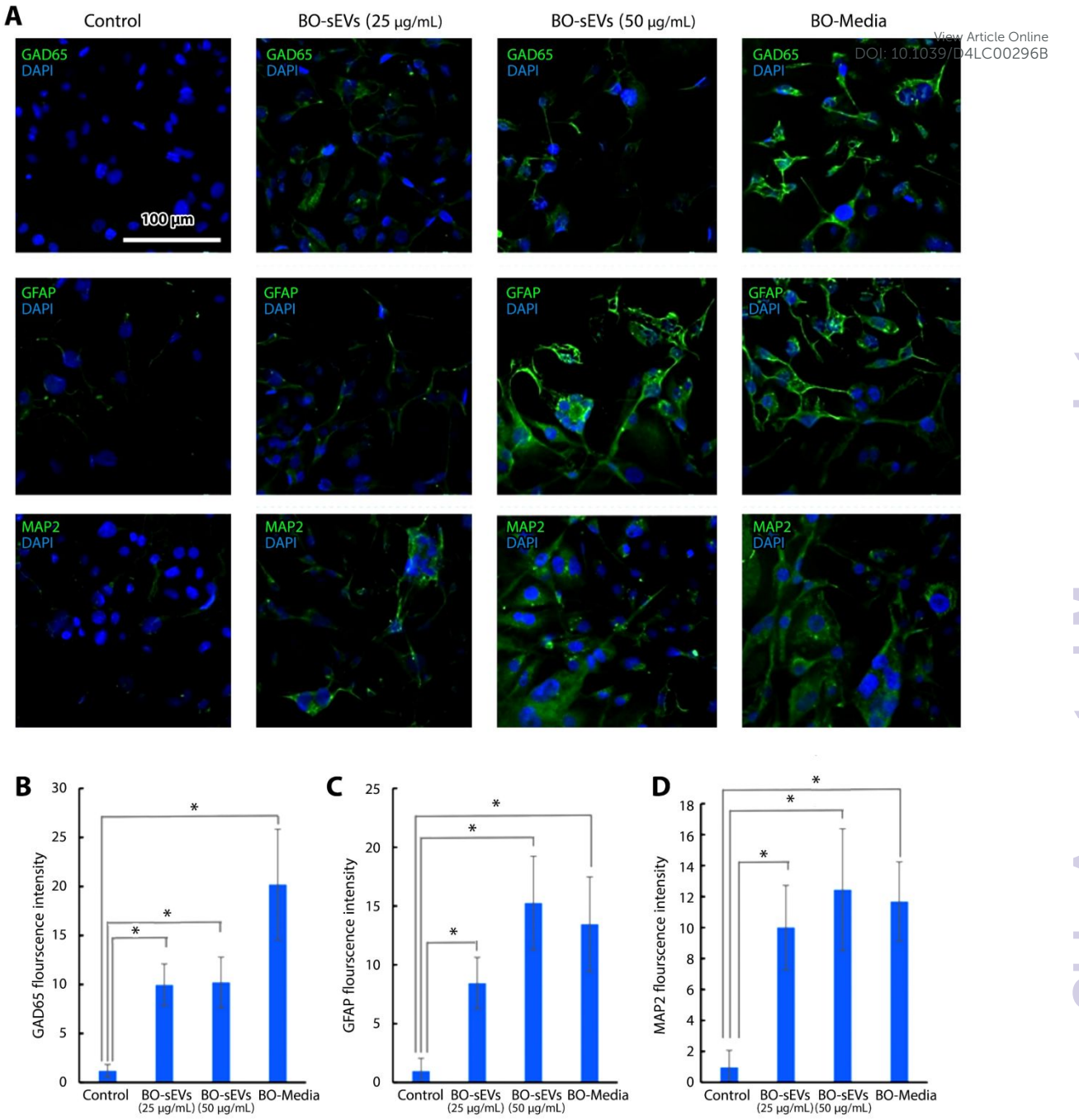

Figure 7. *(A) Confocal microscopy of MDA-MB-231 cells treated with PBS, BO-sEVs and BO-Media. Quantification of confocal images for expression levels of GAD65 (B), GFAP (C), and MAP2 (D) in MDA-MB-231 cells treated with varying concentrations of BO-sEVs and BO-Media(*p < 0.05).*

3.8 Effect of BO-sEVs on Proteomics of Breast Carcinoma Cells

The effect of BO-sEVs was assessed on the protein expression of MDA-MB-231 cells using mass spectrometry. Heatmap visualization of average linkage clustering and Euclidean distance measurement techniques were employed to analyse the protein expression levels in MDA-MB-231 cells post a 24-hour treatment period with PBS (control), BO-sEVs, and brain organoid media. The proteomics data showed that 1899 distinct proteins were identified across groups. To identify significantly altered proteins, we applied the following criteria: a fold change threshold of ≥1.6 for upregulation and ≤0.6 for downregulation when comparing the treated groups to the control group. Additionally, a significance threshold of $p < 0.05$ was utilized to ensure the statistical significance of the observed differences in protein expression levels. Our results showed that in the BO-sEVs group,

100 and 600 proteins were respectively upregulated and downregulated in comparison to control. In the brain organoid media group, 124 and 339 proteins were respectively upregulated and downregulated. For a focused analysis and to construct a manageable heatmap, we prioritized proteins based on their -Log10 p-value, ultimately selecting the top 90 proteins for inclusion in the heatmap. As shown in the heatmap (Figure 8), in MDA-MB-231 cells treated with BO-sEVs, proteins such as TBB2A, MYH10, EF1A2, XPO2, LMNA, TBB5, DYHC1, SPTB2, MYOF, and ANXA6 showed the most significant increases in expression levels, while proteins such as TBA4A, G3P, ALDOA, PGK1, TKT, EZRI, CAP1, EF2, MOES, PDIA6, and ENOA exhibited the most substantial decrease (Figure 8A). The proteins that exhibited the greatest increase and decrease among all identified proteins following treatment with BO-sEVs and media are depicted in Figures 8B and 8C.

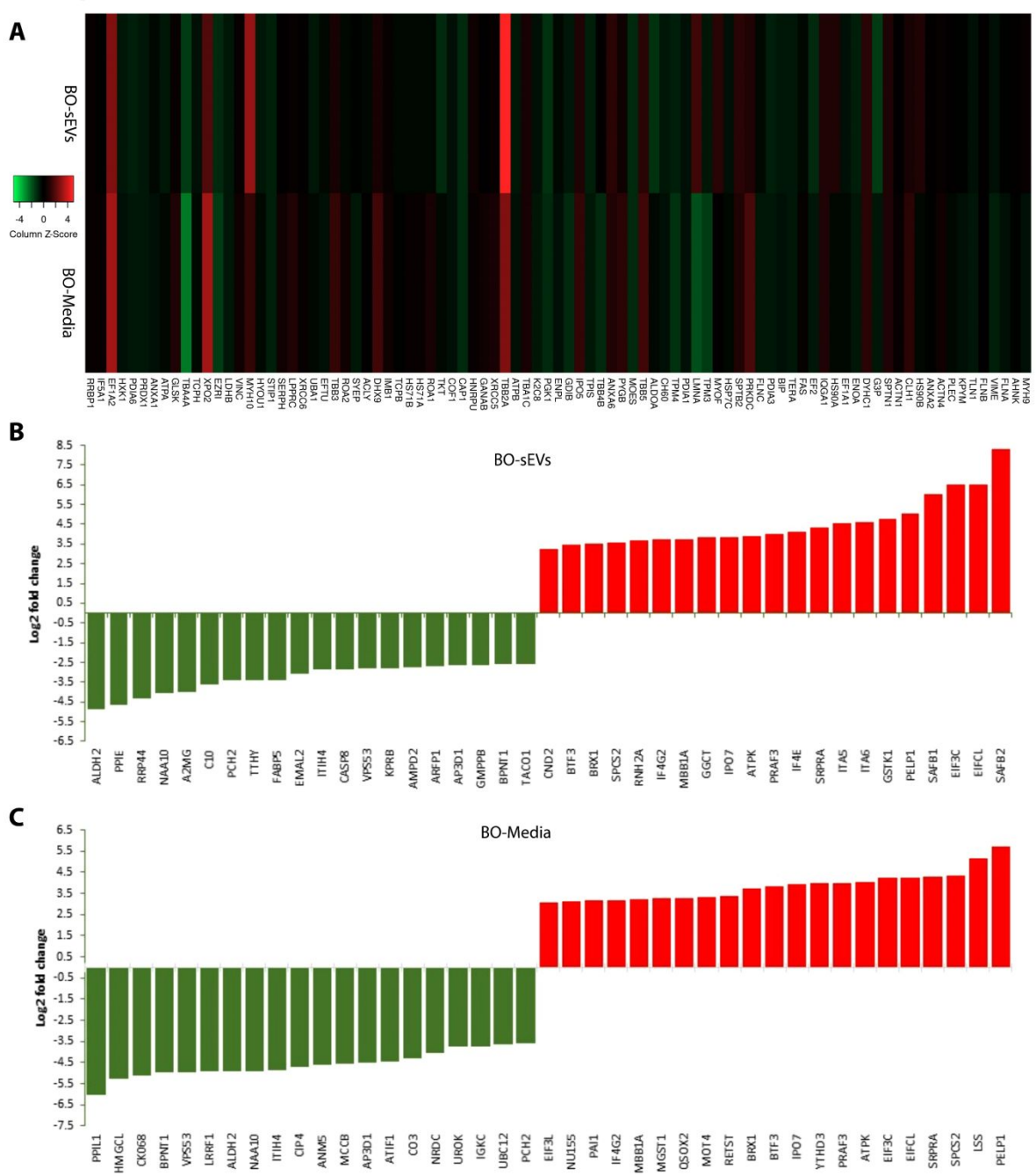

Figure 8. Quantitative proteomic analysis of MDA-MB-231 cells treated with BO-sEVs and BO-Media after 24 hours. A) Heatmap of the first 90 proteins based on the -log P-value. B) The top proteins among the 1799 proteins that were upregulated (red) and downregulated after treatment with BO-sEVs and BO-Media. C) proteins with the most significant changes after treatment with BO-sEVs and media.

3.9 Effect of BO-sEVs on Cytokine production by Breast Carcinoma Cells

Cytokine profiling was performed on sEVs of BO-sEVs treated MDA-MB-231 using a cytokine antibody profiling array. Our results demonstrated a significant increase in the expression levels of certain cytokines-, including Monocyte Chemoattractant Protein-1 (MCP-1), interleukin-6 (IL-6), IL-8, IL-10, Growth-Regulated Oncogene (GRO), and Growth-Regulated Oncogene-alpha (GRO-α), in response to exposure to BO-sEVs. These alterations in cytokine expression reflect a potential modulation of signaling pathways, immune responses, and inflammatory processes (Figure 9A-D). The results also show a significantly increased production of IL-6, angiogenin, and VEGF in BO-Media-treated MDA-MB-231 carcinoma cells compared to the control and BO-sEVs groups (Figure 9D).

Elevated MCP-1 levels might suggest increased recruitment of monocytes and macrophages, potentially impacting immune cell dynamics within the brain microenvironment during metastatic adaptation caused by brain sEVs. The upregulation of IL-6 can be associated with pro-inflammatory responses, angiogenesis, and immune evasion. GRO and GRO-alpha are known to stimulate cell migration and invasion [39].

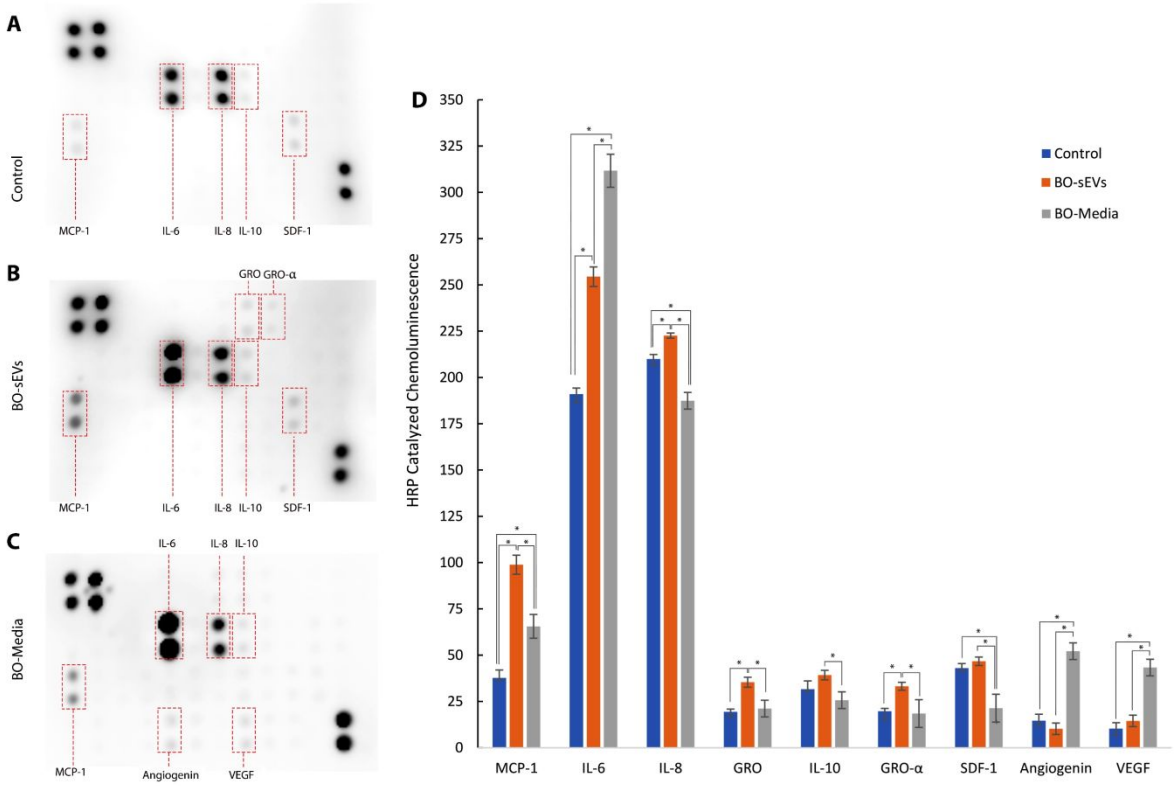

Figure 9. (A-B) *Micrographs depicting cytokine profiling performed on the culture medium retrieved from (A) PBS treated, (B) BO-sEVs-treated, and (C) BO-Media-treated MDA-MB-231 cells. (C) Quantitative analysis of HRP-catalyzed chemiluminescence of cytokine membranes using ImageJ software shows a significant increase in MCP-1, IL-6, IL-8, IL-10, GRO, and GRO-α after treatment with BO-sEVs (*p < 0.05).*

3.10 Effect of BO-sEVs on 3D Migration of MDA-MB-231 Cells

To study the potential of sEVs in enhancing the 3D migratory properties of carcinoma cells, MDA-MB-231 cells were first treated with BO-sEVs for 48 hours in an FBS-free medium. BO-sEVs significantly increased the migration of MDA-MB-231 cells through the collagen I gel. Subsequently, a three-channel microfluidic device was utilized to create a 'brain organoid on a chip' co-cultured with MDA-MB-231 cells under various conditions (control, educated with BO-sEVs, and BO-Media (Figure 10A). Brain organoids were introduced in the middle channel and simultaneously co-cultured with both educated groups and controls (Figure 10 A). The AIM Biotech device enabled a co-culture of early brain organoids (day 10) encapsulated in a collagen hydrogel (in the middle channel) with MDA-MB-

View Article Online
DOI: 10.1039/D4LC00296B

231 cells, as well as MDA-MB-231 cells pre-treated with brain organoid media (in the lateral channels) (Figure 10A).

Before starting the co-culture experiment, the viability of brain organoids after 24 hours through collagen in microfluidic devices was assessed using a live/dead staining method. The results demonstrate that the majority of cells within the organoids remained viable, as indicated by intense green fluorescence, with minimal red fluorescence observed, indicating a low level of cell death (Figure 10B).

Our findings revealed that MDA-MB-231 cell pre-treatment with BO-sEVs enhanced the migration of MDA-MB-231 cells inside the 3D hydrogel. Specifically, average invasive distance of MDA-MB-231 cells in control group (137.100 ± 47.170 µm), increased to 167.36 ± 56.26 µm (Figure 10C-D). We then investigated whether the BO-Media could also increase the invasive behaviour of carcinoma cells. In our co-culture system, MDA-MB-231 cells, without pre-treatment, displayed an average invasive distance of 127.89 ± 52.761 µm from the gel's surface (Figure 10C-D). Conversely, MDA-MB-231 cells pre-treated with brain organoid media exhibited an augmented invasive response, with an average distance of 189.830 ± 63.88 µm.

Our results indicated that, across both pre-treatment groups, the average migration distance was significantly higher than that of the control group. Brain organoid media pre-treatment enhanced the invasive potential of MDA-MB-231 cells to a greater extent than sEVs, although the difference was not significant. Despite numerical variations, the overall invasion patterns were reproducible. Moreover, the controls (MDA-MB-231 cells) in both groups exhibited almost identical results in terms of migration distance. Furthermore, immunostaining of MDA-MB-231 cells inside device showed that the BO-sEVs increase the vimentin expression significantly compared to the control reflecting changes in mesenchymal characteristics inside chip (Figure 10 E-F).

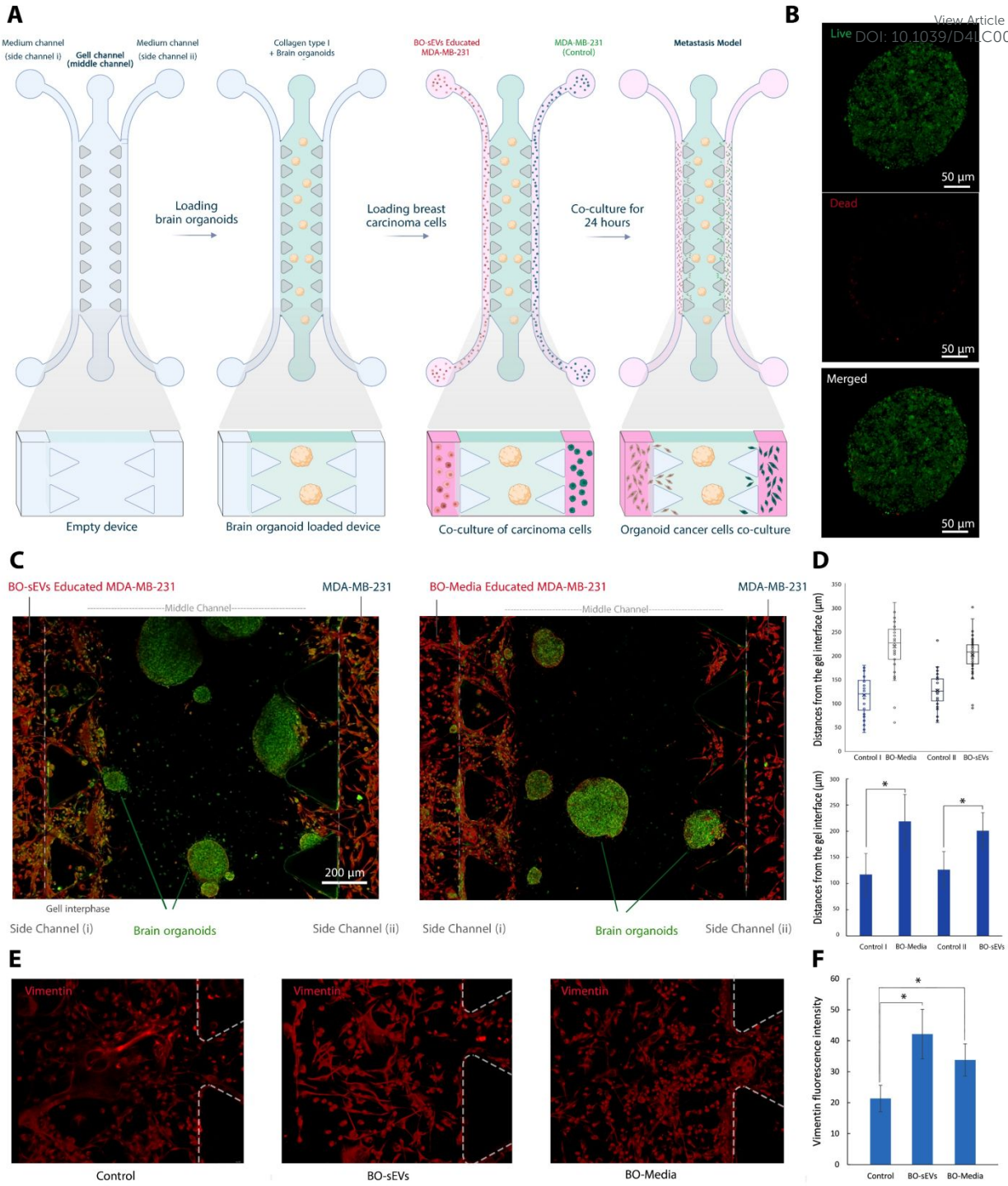

Figure 10. *(A) Schematic of compartments of microfluidic device and step by step developing of microfluidic-based co-culture system for studying the role of BO-sEVs and BO-Media in metastasis of MDA-MB-231 cells toward brain organoids. (B) live (green, Calcein AM) and dead (read, Ethidium homodimer-1) imaging of brain organoids encapsulated through collagen type I inside microfluidic device after 24 hours. (C) Confocal microscopy images from the co-culture setup within microfluidic devices. Brain organoids (green, Pax6) were co-cultured in the middle channel, while MDA-MB-231 cells (red, vimentin, right) and brain organoid media-treated MDA-MB-231 cells (red, vimentin, left) were cultured in the side channels (Scale bar: 200 µm). D) Quantification of confocal images for migration of MDA-MB-231 cells through hydrogel treated with PBS (control), BO-sEVs and BO-Media (*p < 0.05). (E) Immunostaining images showing the expressions of vimentin in MDA-MB-231 cells treated with PBS (control), BO-sEVs, and BO-Media after 24 hours. Mean fluorescence analysis showed that BO-sEVs significantly increased the expression of vimentin in breast carcinoma cells (*p < 0.05).*

View Article Online
DOI: 10.1039/D4LC00296B

4. Discussion

Colonization of the brain by circulating breast carcinoma cells is promoted by the soil to confer the seeds to survive and develop in a hostile environment [30]. Breast carcinoma cells can adapt to this new environment through cell-cell communications such as gap junctions and other intercellular contacts, soluble factors such as cytokines, growth factors, and hormones, and sEVs-based communications [40, 41]. In this study, we investigated the impact of BO-sEVs to promote adaptation to proliferate, and to acquire aggressiveness allowing breast carcinoma cells to acquire stem-like properties and to invade the brain.

We utilized brain organoids as the source of sEVs, at variance from previous research that relied on sEVs isolated from differentiated astrocytes cultured on 2D surfaces [27, 29, 31]. In this project, we isolated sEVs from highly mature embryonic stem cell-derived brain organoids expressing neuronal and astrocyte markers. Brain organoids offer a three-dimensional representation of the brain's complexity, microenvironment, and interactions, making them a surrogate of brain tissue as a source of sEVs [23, 24]. Our confocal imaging data confirmed the presence of astrocytes within the 3D structure of brain organoids, networking with neurons. While BO-sEVs have been reported in a few studies, their characterizations remain incomplete. sEVs isolated from induced forebrain neural progenitor cortical organoids were loaded with superparamagnetic iron oxide nanoparticles for imaging purposes [42]. Ji *et al.* the neuroprotective effects were compared using either cerebral organoids (60-140 days) or mesenchymal stem cell-derived sEVs on astrocytes [43]. Herein, the isolation of BO-sEVs was performed using the gold standard method of ultracentrifugation [44]. Results from TEM and NTA confirmed the sEVs' size distribution, spherical morphology, and concentration. Additionally, the presence of tetraspanins glycoproteins CD9, CD63, and CD81 on their surface was confirmed using western blotting [45]. Western blotting also revealed the presence of the GLAST protein, a known marker for dendritic sEVs, further confirming neural differentiation and maturation within the brain organoids [46-48]. GLAST has been identified as a marker in astrocyte-derived sEVs [49]. The proteomics analysis of BO-sEVs reveals the expression of a variety of proteins connected to nervous system development and some of the proteins associated with the growth and metastasis of TNBC. Some proteins are involved in the maintenance of the brain functions, controlling inflammation, and stress. For instance, NEP (Neprilysin), an integral membrane-bound metallopeptidase responsible for cleaving amyloid β (Aβ) peptide is crucial for brain development and function [50]. PRDX6 (Peroxiredoxin 6) is an antioxidant enzyme that helps protect neural cells from oxidative stress [51], and ANXA1 (Annexin A1) is involved in modulating inflammation in the brain [52].

The uptake of organoid-derived sEVs labelled with PKH-67 by MDA-MB-231 cells was monitored after 24 hours, a time previously used in the literature [53]. After confirming the internalization of sEVs by breast carcinoma cells, proliferation was assessed in different pre-treatments 24 hours with PBS, Brain Organoid sEVs, or Brain Organoid Media. The group treated with BO-sEVs did not proliferate faster as compared to the control group on day 1. However, by day 2 and day 3, the sEVs Pre-Treatment group exhibited slower growth compared to the other group. These results, along with Ki-67 staining results, suggest that the presence of sEVs from brain organoids may have an inhibitory effect on the growth of MDA-MB-231 cells. These results are compatible with other studies that have highlighted a reduced proliferation of breast carcinoma cells cocultured with different neural cell types [54]. The scratch test also suggested that BO-sEVs can promote the wound closure capacity of breast carcinoma cells. BO-sEVs revealed a reduction in cell roundness and an increase in cell elongation, suggesting an enhanced migratory phenotype.

BO-sEVs enhance spheroid formation and stemness in MDA-MB-231 carcinoma cells. BO-sEVs also increase spheroidogenesis, promote EMT and invasiveness of carcinoma cells toward brain organoids. To further explore this potential link, we investigated the expression of E-cadherin, the landmark marker of adherens junctions in epithelial cells [55]. The reduction in E-cadherin expression in the presence of BO-sEVs indicates a shift from the epithelial phenotype toward a more mesenchymal state. Additionally, the overexpression of CD44, a cell surface glycoprotein associated with the

View Article Online
DOI: 10.1039/D4LC00296B

stemness of carcinoma cells, in MDA-MB-231 cells suggests a more aggressive phenotype in carcinoma cells within MDA-MB-231 spheroids [56].

The impact of BO-sEVs on the expression of PD-L1, CD49f, vimentin, and EGFR was analysed in the MDA-MB-231 cell line. These markers provide an essential information on breast cancer progression, therapeutic responsiveness, and potential therapeutic targets in the clinic [57]. The BO-sEVs group enhanced PD-L1 expression in MDA-MB-231 cells, indicating potential modulation of immune responses. PD-L1 is known for its role in immune checkpoint regulation and its ability to facilitate tumor immune evasion [58, 59]. The overexpression of PD-L1 in TNBC patients prompted the use of checkpoint inhibitors a target of in TNBC patients [60, 61]. A study revealed an association between increased PD-L1 expression in human TNBCs and the presence of stem-like and immune-related characteristics [62]. Similarly, CD49f (integrin alpha 6) expression was markedly elevated in the BO-sEVs group, suggesting potential increase in chemoresistance and stemness of breast carcinoma cells [63]. CD49f is also associated with cell adhesion of cancer stem cells ensuring their interaction with the extracellular matrix [64]. This marker is known as a breast cancer stem cell marker that has been correlated with distant metastasis, including brain metastasis [65, 66]. Studies showed that in initially sensitive TNBC tumours, a population of CD49f+ cells within the tumor-initiating population exhibited increased resistance to the taxane family of chemotherapeutic drugs [67, 68]. Furthermore, the BO-sEVs group showed a significant increase in vimentin expression, potentially reflecting in the enforcement of mesenchymal characteristics [69]. Vimentin is a cytoskeletal protein associated with the mesenchymal phenotype and increased motility in carcinoma cells [70]. This observation implies that sEVs from brain organoids may contribute to the acquisition of mesenchymal traits by TNBC cells, potentially enhancing their aggressiveness and chemotherapy resistance [69, 71].

Studies showed that biopsies from brain metastasis of breast carcinoma cells express some characteristics of neural cells [72-74]. This neural mimicry of breast carcinoma cells could favour colonization in the brain. For instance, breast carcinoma cells can express GAD 65/GAD67 enzymes involved in the synthesis of GABA, a major inhibitory neurotransmitter in the central nervous system [72]. [73, 74]. In another study, Neman *et al.* reported that breast carcinoma cells in brain metastases exhibited a GABAergic phenotype similar to neurons, indicating their adaptation to the neural environment for metastasis [32]. Herein, we showed that BO-sEVs enhance the expression of glial (GFAP) and neuronal markers (MAP-2) in MDA-MB-231 cells. GFAP is an intermediate filament protein specific to astrocytes that plays supportive structural and functional roles in the brain and spinal cord [75, 76]. Human tissue samples and *in vivo* studies show that metastatic breast carcinoma cells adjacent to astrocytes surrounding the tumor and within the tumor express this glial marker, GFAP [32]. This astrocyte-like behaviour is the result of a reciprocal interaction between breast carcinoma cells and astrocytes and can increase brain tropism, metastasis, and colonization [77]. The microtubule-associated protein 2 (MAP-2) is a protein that is primarily found in the cytoskeleton of neurons in the central nervous system [78, 79]. Studies showed that the enhanced expression of MAP-2 in breast carcinoma cells also increases their sensitivity to some chemotherapeutic drugs, such as paclitaxel [80, 81].

The proteomics analysis revealed differences in protein expression in MDA-MB-231 cells after treatment with brain organoid sEVs. Among the top 90 proteins with the highest expression, a specific isoform of tubulin (tubulin beta-2A chain, TBB2A or TUBB2A) had the highest upregulation. TUBB2A is highly expressed mainly in brain and plays an important role in neurite outgrowth[82]. This protein is also expressed in breast epithelial cells and studies shows that it can plays a crucial role in distant metastasis and drug resistance in breast cancers[83, 84]. TUBB2A regulates the dynamics of microtubules in carcinoma cells and is in interaction with PI3K/AKT and MAPK signalling pathways leading to enhanced survival of carcinoma cells. Using advanced proteomics, Shin *et al.* identified TUBB2A as a novel biomarker for distant metastasis in TNBC [85]. This research revealed that TUBB2A expression correlates with distant metastatic potential in TNBC [85]. Another report showed that TUBB2A is highly expressed in TNBC and negatively correlated with T cell recruitment in the cancer-immunity cycle, suggesting its role in poor prognosis and potential as a therapeutic target in TNBC [86]. Studies also shows that the expression of tubulin family proteins, as brain-associated proteins, plays a crucial role in brain metastasis of breast cancers [87]. MYH10 (myosin heavy chain ten or non-muscle myosin IIB) is another protein that significantly increased. Myosin IIA and IIB isoforms are critical for cell migration

View Article Online
DOI: 10.1039/D4LC00296B

in MDA-MB-231 breast carcinoma cells, with myosin IIB playing a preferential role in lamellar protrusion mechanics during cell spreading on fibronectin [88]. Studies also showed that upregulation of MYOF (Myoferlin) and ANXA6 (annexin A6) can lead to more invasiveness, apoptosis, and drug resistance [89, 90]. The downregulation of TBA4A (Tubulin Alpha 4a), EZRI (Ezrin), and MOES (Moesin) impacts structural integrity and cell motility. Additionally, decreased G3P (glycerol-3-phosphate dehydrogenase (G3PDH)), ALDOA (Aldolase A), PGK1 (Phosphoglycerate Kinase 1), and ENOA (Enolase 1) can be related to altered energy metabolism and glycolysis in carcinoma cells [91-94].

The cytokine profiling arrays showed a significant increase in the secretion of MCP-1, IL-6, IL-8, IL-10, GRO (Growth-Regulated Oncogene), and GRO-α by MDA-MB-231 cells in response to exposure to brain organoid-derived factors. MCP-1, also known as chemokine ligand 2, CCL2, is one of the key chemokines that regulate the migration and infiltration of monocytes and tumor-associated macrophages. MCP-1 is also implicated in breast cancer progression, and blocking CCL2 with neutralizing antibodies decreased macrophage infiltration and tumor growth in a mouse model of breast cancer [95]. The targeted gene silencing of CCL2 in TNBC inhibited primary tumor growth and metastasis in animal models through reduced cancer stem cell renewal and recruitment of M2 macrophages [96]. Studies show that CCL2 negatively regulates breast cancer metastasis to bone while promoting metastasis to the brain and lung [97, 98]. In brain metastasis, CCL2 is found to facilitate breast cancer cell recruitment to the brain and is associated with PTEN loss and activation of NF-κB [19]. In breast cancer, an enhanced level of IL-6 is associated with reduced patient survival, accelerated cell proliferation, invasion, metastasis, and angiogenesis in tumor sites through different signaling pathways [99, 100]. Additionally, the upregulation of the IL-10 cytokine can lead to the diminishing host microenvironment immune response during tumorigenesis [101]. IL-8 (CXCL8), a pro-inflammatory protein, plays different roles in inducing invasiveness and dampening the immune system in the tumor site. CXCL8 was significantly upregulated in TNBC brain metastasis tissue samples and a TNBC brain metastasis cell line [102]. Our results also revealed that the expression of GRO proteins, including GRO-α (CXCL1), is enhanced in MDA-MB-231 cells. Previous studies show that these markers play essential roles in triple-negative breast carcinoma cells ' invasive and metastatic behaviour [39].

We compared the role of BO-sEVs' pre-treatment on the 3D migration of MDA-MB-231 cells inside a three-unit co-culture microphysiological system. Our results confirmed the inducing role of BO-sEVs in the pronounced migration of a majority of MDA-MB-231 cells. Other studies have also shown the positive impact of a soil-seed co-culture system on organotropism and organ adaptation of carcinoma cells; however, these studies were carried out in 2D. The role of astrocyte-derived sEVs has been investigated in 2D culture systems [27, 29, 31]. Interestingly, our results showed that BO-sEVs treatment could have a similar effect on the invasive behaviour as brain organoid supernatant medium. This study provides the first exploration of brain organoids within a 3D microenvironment to study soil-derived sEVs' role in TNBC metastasis. Previous studies have mainly employed various brain cell types in devices as brain models [103, 104]. A recent survey reported the effects of hormone-positive breast cancer cell-derived sEVs on the early neurodevelopment of brain organoids within an array of micropillar chips [105]. For future studies, incorporating vascular lumens or vascularization into brain organoids-on-a-chip models can enhance their mimicking capability [104]. In addition, characterizing the sEVs from brain-educated carcinoma cells can provide valuable information for liquid biopsy to improve predictive medicine.

The multifaceted effects of BO-sEVs on TNBC cell-line behaviour underscore the need for further investigations into the role of sEVs in the metastatic process. These findings offer valuable insights into potential therapeutic targets for mitigating brain metastasis in TNBC and highlight the significance of organ-specific adaptations in the metastatic cascade. Future studies may explore the clinical implications of these findings for developing targeted therapies for TNBC patients at risk of brain metastasis.

5. Conclusion

View Article Online
DOI: 10.1039/D4LC00296B

In summary, our findings reveal the complex impact of BO-sEVs on TNBC cell line (MDA-MB-231) behaviour, encompassing alterations in proliferation, invasiveness, stemness, immune responses, and cell secretion properties. Furthermore, these sEVs promote neural -like differentiation marker expression in the carcinoma cells and increased their invasion in a 3D environment toward brain organoids inside a microphysiological system. These results offer valuable insights into the interaction between soil-derived sEVs and TNBC, opening new avenues for research and potential therapeutic strategies in the diagnosis and treatment of this aggressive breast cancer subtype.

6. Acknowledgments:

We acknowledge the support of the Cancer Institute NSW through Career Development Fellowships (2021/CDF1148) (M.E.W.). The authors also wish to thank Dr. Sareh Zhand supporting the cytokine profiling array analysis.

7. Conflict of Interest

The authors declare no conflict of interest.

8. References

1. Y. Lv, X. Ma, Y. Du and J. Feng, *Onco Targets Ther.*, 2021, 589-607.
2. G. Bianchini, C. De Angelis, L. Licata and L. Gianni, *Nature reviews Clinical oncology*, 2022, **19**, 91-113.
3. P. Zagami and L. A. Carey, *NPJ Breast Cancer*, 2022, **8**, 95.
4. M. Kuksis, Y. Gao, W. Tran, C. Hoey, A. Kiss, A. S. Komorowski, A. J. Dhaliwal, A. Sahgal, S. Das and K. K. Chan, *Neuro Oncol.*, 2021, **23**, 894-904.
5. S. Dawood, X. Lei, J. K. Litton, T. A. Buchholz, G. N. Hortobagyi and A. M. Gonzalez-Angulo, *Cancer*, 2012, **118**, 4652-4659.
6. S. Paget, *The Lancet*, 1889, **133**, 571-573.
7. I. Wortzel, S. Dror, C. M. Kenific and D. Lyden, *Dev. Cell*, 2019, **49**, 347-360.
8. A. Hoshino, B. Costa-Silva, T.-L. Shen, G. Rodrigues, A. Hashimoto, M. Tesic Mark, H. Molina, S. Kohsaka, A. Di Giannatale and S. Ceder, *Nature*, 2015, **527**, 329-335.
9. A. Möller and R. J. Lobb, *Nature Reviews Cancer*, 2020, **20**, 697-709.
10. L. Cheng and A. F. Hill, *Nature Reviews Drug Discovery*, 2022, **21**, 379-399.
11. G. Van Niel, G. d'Angelo and G. Raposo, *Nature reviews Molecular cell biology*, 2018, **19**, 213-228.
12. L. Milane, A. Singh, G. Mattheolabakis, M. Suresh and M. M. Amiji, *Journal of Controlled Release*, 2015, **219**, 278-294.
13. Y. Tan, X. Luo, W. Lv, W. Hu, C. Zhao, M. Xiong, Y. Yi, D. Wang, Y. Wang and H. Wang, *Cell Death Dis.*, 2021, **12**, 547.
14. X. Wang, L. Tian, J. Lu and I. O.-L. Ng, *Oncogenesis*, 2022, **11**, 54.
15. Q. Liu, F. Peng and J. Chen, *Int. J. Mol. Sci.*, 2019, **20**, 3884.
16. M. Osaki and F. Okada, *Yonago Acta Med.*, 2019, **62**, 182-190.

17. G. Rodrigues, A. Hoshino, C. M. Kenific, I. R. Matei, L. Steiner, D. Freitas, H. S. Kim, P. R. Oxley, I. Scandariato and I. Casanova-Salas, *Nat. Cell Biol.*, 2019, **21**, 1403-1412.
18. J. Huang, M. Shen, M. Yan, Y. Cui, Z. Gao and X. Meng, *Acta Biochimica et Biophysica Sinica*, 2019, **51**, 900-907.
19. L. Zhang, S. Zhang, J. Yao, F. J. Lowery, Q. Zhang, W.-C. Huang, P. Li, M. Li, X. Wang and C. Zhang, *Nature*, 2015, **527**, 100-104.
20. J. Fares, A. Cordero, D. Kanojia and M. S. Lesniak, *Cancers (Basel)*, 2021, **13**, 142.
21. R. Jandial, C. Choy, D. M. Levy, M. Y. Chen and K. I. Ansari, *Clin. Exp. Metastasis*, 2017, **34**, 185-196.
22. M. Han, H. Yang, X. Lu, Y. Li, Z. Liu, F. Li, Z. Shang, X. Wang, X. Li and J. Li, *Nano Lett.*, 2022, **22**, 6391-6401.
23. I. Chiaradia and M. A. Lancaster, *Nat. Neurosci.*, 2020, **23**, 1496-1508.
24. A.-N. Cho, Y. Jin, Y. An, J. Kim, Y. S. Choi, J. S. Lee, J. Kim, W.-Y. Choi, D.-J. Koo and W. Yu, *Nature communications*, 2021, **12**, 4730.
25. E. Di Lullo and A. R. Kriegstein, *Nature Reviews Neuroscience*, 2017, **18**, 573-584.
26. S. Kim, A. N. Cho, S. Min, S. Kim and S. W. Cho, *Advanced Therapeutics*, 2019, **2**, 1800087.
27. Q. Chen, A. Boire, X. Jin, M. Valiente, E. E. Er, A. Lopez-Soto, L. S Jacob, R. Patwa, H. Shah and K. Xu, *Nature*, 2016, **533**, 493-498.
28. D. Wasilewski, N. Priego, C. Fustero-Torre and M. Valiente, *Front. Oncol.*, 2017, **7**, 298.
29. Q. Zeng, I. P. Michael, P. Zhang, S. Saghafinia, G. Knott, W. Jiao, B. D. McCabe, J. A. Galván, H. P. Robinson and I. Zlobec, *Nature*, 2019, **573**, 526-531.
30. L. K. Boroughs and R. J. DeBerardinis, *Nat. Cell Biol.*, 2015, **17**, 351-359.
31. J. A. Stogsdill, J. Ramirez, D. Liu, Y. H. Kim, K. T. Baldwin, E. Enustun, T. Ejikeme, R.-R. Ji and C. Eroglu, *Nature*, 2017, **551**, 192-197.
32. J. Neman, J. Termini, S. Wilczynski, N. Vaidehi, C. Choy, C. M. Kowolik, H. Li, A. C. Hambrecht, E. Roberts and R. Jandial, *Proceedings of the National Academy of Sciences*, 2014, **111**, 984-989.
33. A. Cordero, D. Kanojia, J. Miska, W. K. Panek, A. Xiao, Y. Han, N. Bonamici, W. Zhou, T. Xiao and M. Wu, *Oncogene*, 2019, **38**, 6445-6460.
34. L. Ye, Y. Wu, J. Zhou, M. Xie, Z. Zhang and C. Su, *Biol. Proced. Online*, 2023, **25**, 1-11.
35. K. Ganesh and J. Massague, *Nat. Med.*, 2021, **27**, 34-44.
36. J. Termini, J. Neman and R. Jandial, *Cancer Res.*, 2014, **74**, 4011-4015.
37. A.-N. Cho, F. Bright, N. Morey, C. Au, L. M. Ittner and Y. D. Ke, *Cells*, 2022, **11**, 3194.
38. D. J. Harney, A. T. Hutchison, L. Hatchwell, S. J. Humphrey, D. E. James, S. Hocking, L. K. Heilbronn and M. Larance, *J. Proteome Res.*, 2019, **18**, 2228-2240.
39. K. Bhat, M. Sarkissyan, Y. Wu and J. V. Vadgama, *Oncol. Rep.*, 2017, **38**, 21-30.
40. Y. Kienast, L. Von Baumgarten, M. Fuhrmann, W. E. Klinkert, R. Goldbrunner, J. Herms and F. Winkler, *Nat. Med.*, 2010, **16**, 116-122.
41. E. I. Chen, J. Hewel, J. S. Krueger, C. Tiraby, M. R. Weber, A. Kralli, K. Becker, J. R. Yates III and B. Felding-Habermann, *Cancer Res.*, 2007, **67**, 1472-1486.
42. C. Liu, S. Helsper, M. Marzano, X. Chen, L. Muok, C. Esmonde, C. Zeng, L. Sun, S. C. Grant and Y. Li, *Biomedicines*, 2022, **10**, 3060.
43. X. Ji, S. Zhou, N. Wang, J. Wang, Y. Wu, Y. Duan, P. Ni, J. Zhang and S. Yu, *Int. J. Mol. Sci.*, 2023, **24**, 11048.
44. C. Coughlan, K. D. Bruce, O. Burgy, T. D. Boyd, C. R. Michel, J. E. Garcia-Perez, V. Adame, P. Anton, B. M. Bettcher and H. J. Chial, *Curr. Protoc. Cell Biol.*, 2020, **88**, e110.
45. Y. Fan, C. Pionneau, F. Cocozza, P. y. Boëlle, S. Chardonnet, S. Charrin, C. Théry, P. Zimmermann and E. Rubinstein, *Journal of Extracellular Vesicles*, 2023, **12**, 12352.
46. S. Qadri, A. S. Parray and I. Ahmed, *Journal*, 2022, **16**, 1025277.
47. E. J. Goetzl, J. B. Schwartz, E. L. Abner, G. A. Jicha and D. Kapogiannis, *Ann. Neurol.*, 2018, **83**, 544-552.
48. L. Huo, X. Du, X. Li, S. Liu and Y. Xu, *Front. Neurosci.*, 2021, **15**, 738442.

49. E. J. Goetzl, M. Mustapic, D. Kapogiannis, E. Eitan, I. V. Lobach, L. Goetzl, J. B. Schwartz and B. L. Miller, *The FASEB Journal*, 2016, **30**, 3853.
50. N. Nalivaeva, I. Zhuravin and A. Turner, *Mech. Ageing Dev.*, 2020, **192**, 111363.
51. J. Liao, Y. Zhang, X. Chen and J. Zhang, *Mol. Neurobiol.*, 2021, **58**, 4348-4364.
52. S. McArthur, E. Cristante, M. Paterno, H. Christian, F. Roncaroli, G. E. Gillies and E. Solito, *The Journal of Immunology*, 2010, **185**, 6317-6328.
53. S. Pan, X. Zhao, C. Shao, B. Fu, Y. Huang, N. Zhang, X. Dou, Z. Zhang, Y. Qiu and R. Wang, *Cell Death Dis.*, 2021, **12**, 38.
54. J. Neman, C. Choy, C. M. Kowolik, A. Anderson, V. J. Duenas, S. Waliany, B. T. Chen, M. Y. Chen and R. Jandial, *Clin. Exp. Metastasis*, 2013, **30**, 753-768.
55. M. Saitoh, *The Journal of Biochemistry*, 2018, **164**, 257-264.
56. C. Chen, S. Zhao, A. Karnad and J. W. Freeman, *J. Hematol. Oncol.*, 2018, **11**, 1-23.
57. T. Saha and K. E. Lukong, *Front. Oncol.*, 2022, **12**, 856974.
58. P. Dong, Y. Xiong, J. Yue, S. J. Hanley and H. Watari, *Front. Oncol.*, 2018, **8**, 386.
59. L. Chen and X. Han, *The Journal of clinical investigation*, 2015, **125**, 3384-3391.
60. M. Nakhjavani and S. Shigdar, *Pharmacol. Res.*, 2022, **175**, 106019.
61. M. Nakhjavani and S. Shigdar, *Cancers (Basel)*, 2022, **14**, 6258.
62. L. Castagnoli, V. Cancila, S. L. Cordoba-Romero, S. Faraci, G. Talarico, B. Belmonte, M. V. Iorio, M. Milani, T. Volpari and C. Chiodoni, *Oncogene*, 2019, **38**, 4047-4060.
63. I. Velázquez-Quesada, A. J. Ruiz-Moreno, D. Casique-Aguirre, C. Aguirre-Alvarado, F. Cortés-Mendoza, M. de la Fuente-Granada, C. García-Pérez, S. M. Pérez-Tapia, A. González-Arenas and A. Segura-Cabrera, *Drug Des. Devel. Ther.*, 2020, 1799-1811.
64. G. D. Bigoni-Ordóñez, D. Czarnowski, T. Parsons, G. J. Madlambayan and L. G. Villa-Diaz, *Curr. Stem Cell Res. Ther.*, 2019, **14**, 428-436.
65. T. Oskarsson, E. Batlle and J. Massagué, *Cell stem cell*, 2014, **14**, 306-321.
66. A. F. Vieira, A. S. Ribeiro, M. R. Dionísio, B. Sousa, A. R. Nobre, A. Albergaria, A. Santiago-Gómez, N. Mendes, R. Gerhard and F. Schmitt, *Oncotarget*, 2014, **5**, 679.
67. J. Gómez-Miragaya, M. Palafox, L. Paré, G. Yoldi, I. Ferrer, S. Vila, P. Galván, P. Pellegrini, H. Pérez-Montoyo and A. Igea, *Stem cell reports*, 2017, **8**, 1392-1407.
68. J. Gomez-Miragaya and E. González-Suárez, *Molecular & Cellular Oncology*, 2017, **4**, e1338208.
69. E. M. Grasset, M. Dunworth, G. Sharma, M. Loth, J. Tandurella, A. Cimino-Mathews, M. Gentz, S. Bracht, M. Haynes and E. J. Fertig, *Sci. Transl. Med.*, 2022, **14**, eabn7571.
70. K. Vuoriluoto, H. Haugen, S. Kiviluoto, J. Mpindi, J. Nevo, C. Gjerdrum, C. Tiron, J. Lorens and J. Ivaska, *Oncogene*, 2011, **30**, 1436-1448.
71. M. Winter, S. Meignan, P. Völkel, P.-O. Angrand, V. Chopin, N. Bidan, R.-A. Toillon, E. Adriaenssens, C. Lagadec and X. Le Bourhis, *Cells*, 2021, **10**, 1504.
72. Y. Yang, L. Ren, W. Li, Y. Zhang, S. Zhang, B. Ge, H. Yang, G. Du, B. Tang and H. Wang, *Biomed. Pharmacother.*, 2023, **161**, 114410.
73. M. Mazurkiewicz, A. Opolski, J. Wietrzyk, C. Radzikowski and Z. Kleinrok, *Journal of experimental & clinical cancer research: CR*, 1999, **18**, 247-253.
74. D. Zhang, X. Li, Z. Yao, C. Wei, N. Ning and J. Li, *Cancer Lett.*, 2014, **348**, 100-108.
75. J. Middeldorp and E. Hol, *Prog. Neurobiol.*, 2011, **93**, 421-443.
76. A. Abdelhak, M. Foschi, S. Abu-Rumeileh, J. K. Yue, L. D'Anna, A. Huss, P. Oeckl, A. C. Ludolph, J. Kuhle and A. Petzold, *Nature Reviews Neurology*, 2022, **18**, 158-172.
77. D. P. Fitzgerald, D. Palmieri, E. Hua, E. Hargrave, J. M. Herring, Y. Qian, E. Vega-Valle, R. J. Weil, A. M. Stark and A. O. Vortmeyer, *Clin. Exp. Metastasis*, 2008, **25**, 799-810.
78. R. A. DeGiosio, M. J. Grubisha, M. L. MacDonald, B. C. McKinney, C. J. Camacho and R. A. Sweet, *Front. Mol. Neurosci.*, 2022, **15**, 974890.
79. L. Dehmelt and S. Halpain, *Genome Biol.*, 2005, **6**, 1-10.
80. J. A. Bauer, A. B. Chakravarthy, J. M. Rosenbluth, D. Mi, E. H. Seeley, N. De Matos Granja-Ingram, M. G. Olivares, M. C. Kelley, I. A. Mayer and I. M. Meszoely, *Clinical Cancer Research*, 2010, **16**, 681-690.

View Article Online
DOI: 10.1039/D4LC00296B

81. K. Nishio, H. Arioka, T. Ishida, H. Fukumoto, H. Kurokawa, M. Sata, M. Ohata and N. Saijo, *Int. J. Cancer*, 1995, **63**, 688-693.
82. L. J. Leandro-García, S. Leskelä, I. Landa, C. Montero-Conde, E. López-Jiménez, R. León, A. Cascón, M. Robledo and C. Rodríguez-Antona, *Cytoskeleton*, 2010, **67**, 214-223.
83. M. A. Kamal, M. H. Al-Zahrani, S. H. Khan, M. H. Khan, H. A. Al-Subhi, A. Kuerban, M. Aslam, F. A. Al-Abbasi and F. Anwar, *Curr. Drug Metab.*, 2020, **21**, 178-185.
84. T. T. Maliekal, D. Dharmapal and S. Sengupta, *Front. Immunol.*, 2022, **13**, 876278.
85. D. Shin, J. Park, D. Han, J. H. Moon, H. S. Ryu and Y. Kim, *Clin. Proteomics*, 2020, **17**, 1-19.
86. J. Li, J. Yao and L. Qi, *Mol. Biotechnol.*, 2023, 1-14.
87. D. Kanojia, R. A. Morshed, L. Zhang, J. M. Miska, J. Qiao, J. W. Kim, P. Pytel, I. V. Balyasnikova, M. S. Lesniak and A. U. Ahmed, *Mol. Cancer Ther.*, 2015, **14**, 1152-1161.
88. Y. Peng, Z. Chen, Y. He, P. Li, Y. Chen, X. Chen, Y. Jiang, X. Qin, S. Li and T. Li, *Cancer Lett.*, 2022, **524**, 245-258.
89. S. E. Widatalla, O. Y. Korolkova, D. S. Whalen, J. S. Goodwin, K. P. Williams, J. Ochieng and A. M. Sakwe, *Carcinogenesis*, 2019, **40**, 998-1009.
90. S. D. Williams, T. M. Smith, L. V. Stewart and A. M. Sakwe, *Cells*, 2022, **11**, 3007.
91. A. E. Kabakov and V. L. Gabai, *Cells*, 2021, **10**, 3446.
92. Z. Albakova, G. A. Armeev, L. M. Kanevskiy, E. I. Kovalenko and A. M. Sapozhnikov, *Cells*, 2020, **9**, 587.
93. Y. Song, Q. Luo, H. Long, Z. Hu, T. Que, X. a. Zhang, Z. Li, G. Wang, L. Yi and Z. Liu, *Mol. Cancer*, 2014, **13**, 1-12.
94. M. K. Hassan, D. Kumar, S. A. Patel, N. Pattanaik, N. Mohapatra and M. Dixit, *Life Sci.*, 2020, **246**, 117399.
95. H. Fujimoto, T. Sangai, G. Ishii, A. Ikehara, T. Nagashima, M. Miyazaki and A. Ochiai, *Int. J. Cancer*, 2009, **125**, 1276-1284.
96. W. B. Fang, M. Yao, G. Brummer, D. Acevedo, N. Alhakamy, C. Berkland and N. Cheng, *Oncotarget*, 2016, **7**, 49349.
97. M. Takahashi, H. Miyazaki, M. Furihata, H. Sakai, T. Konakahara, M. Watanabe and T. Okada, *Clin. Exp. Metastasis*, 2009, **26**, 817-828.
98. T. Yoshimura, C. Li, Y. Wang and A. Matsukawa, *Cell. Mol. Immunol.*, 2023, 1-25.
99. K. Tawara, H. Scott, J. Emathinger, C. Wolf, D. LaJoie, D. Hedeen, L. Bond, P. Montgomery and C. Jorcyk, *Oncotarget*, 2019, **10**, 2068.
100. S. G. Manore, D. L. Doheny, G. L. Wong and H.-W. Lo, *Front. Oncol.*, 2022, **12**, 866014.
101. C.-M. Chang, H. Y. P. Lam, H.-J. Hsu and S.-J. Jiang, *Tzu-Chi Medical Journal*, 2021, **33**, 203.
102. Y. Shen, B. Zhang, X. Wei, X. Guan and W. Zhang, *Int. Immunopharmacol.*, 2022, **103**, 108454.
103. T. Brown, M. Nowak, A. Bayles, B. Prabhakarpandian, P. Karande, J. Lahann, M. Helgeson and S. Mitragotri, *Journal*.
104. C. Hajal, G. S. Offeddu, Y. Shin, S. Zhang, O. Morozova, D. Hickman, C. G. Knutson and R. D. Kamm, *Nat. Protoc.*, 2022, **17**, 95-128.
105. K. Cui, W. Chen, R. Cao, Y. Xie, P. Wang, Y. Wu, Y. Wang and J. Qin, *Cell Regeneration*, 2022, **11**, 7.